

Review

Recent Advances in Electrospun Nanostructured Electrodes in Zinc-Ion Batteries

Lilin Zhang ¹, **Cong Wei** ¹, **Lin Gao** ², **Meng-Fang Lin** ³, **Alice Lee-Sie Eh** ⁴, **Jingwei Chen** ^{5,*}  and **Shaohui Li** ^{1,*} ¹ School of Materials Science and Engineering, Zhengzhou University, Zhengzhou 450001, China; 23122937r@connect.polyu.hk (L.Z.); weicong@zzu.edu.cn (C.W.)² Hubei Key Laboratory of Energy Storage and Power Battery, School of Mathematics, Physics and Optoelectronic Engineering, Hubei University of Automotive Technology, Shiyan 442002, China; 20230066@huat.edu.cn³ Department of Materials Engineering, Ming Chi University of Technology, New Taipei City 24301, Taiwan; mflin@mail.mcut.edu.tw⁴ Metrohm Singapore Pte Ltd., 31 Toh Guan Road East, #06-08 LW Techno Centre, Singapore 608608, Singapore; alice.eh@metrohm.com.sg⁵ School of Materials Science and Engineering, Ocean University of China, Qingdao 266404, China

* Correspondence: chenjingwei@ouc.edu.cn (J.C.); shaohuili@zzu.edu.cn (S.L.)

Abstract: Zinc-ion batteries (ZIBs) are increasingly recognized as highly promising candidates for grid-scale energy storage systems due to their cost-effectiveness, environmental friendliness, and high security. Despite recent advancements in the research of cathode materials, Zn anodes, and electrolytes, several challenges persist and must be addressed, including cathode dissolution, generation of by-products, and zinc dendrite formation, which hinder the future application of ZIBs. In this review, we systematically summarize the recent developments in electrospinning technology within ZIBs. First, the principle technical parameters and subsequent thermal treatment of electrospinning technology are discussed, and then the synthetic preparation, morphologies, and electrochemical performance of electrospun nanostructured electrodes in ZIBs are comprehensively reviewed. Finally, some perspectives on research directions and optimization strategies for electrospinning technology in energy applications are outlined.



Citation: Zhang, L.; Wei, C.; Gao, L.; Lin, M.-F.; Eh, A.L.-S.; Chen, J.; Li, S. Recent Advances in Electrospun Nanostructured Electrodes in Zinc-Ion Batteries. *Batteries* **2024**, *10*, 22. <https://doi.org/10.3390/batteries10010022>

Academic Editor: Claudio Gerbaldi

Received: 4 December 2023

Revised: 1 January 2024

Accepted: 4 January 2024

Published: 8 January 2024



Copyright: © 2024 by the authors. Licensee MDPI, Basel, Switzerland. This article is an open access article distributed under the terms and conditions of the Creative Commons Attribution (CC BY) license (<https://creativecommons.org/licenses/by/4.0/>).

1. Introduction

In order to address the growing worldwide need for efficient energy storage systems and sustainable development, it is crucial to take the lead in developing affordable, high-capacity, safe, and environmentally friendly batteries [1–3]. Although lithium-ion batteries (LIBs) still dominate the battery storage market, their further application in large-scale and flexible energy storage is impeded by their intrinsic shortages, such as high cost, uneven lithium resources, and the usage of toxic and flammable electrolytes [4–9]. Nonetheless, zinc-ion batteries (ZIBs) are evolving as promising candidates for the next era of energy storage systems due to their economical nature (\$25/kWh), their high ionic conductivity (10^{-1} – 1 S cm $^{-1}$) of aqueous electrolytes, the substantial volumetric capacity (5854 mAh cm $^{-3}$) of Zn anodes, and their exemplary safety features [10–13].

The electrochemical mechanism of ZIBs is similar to that of lithium-ion batteries (LIBs) [14,15], which mainly consists of the insertion/extraction of Zn $^{2+}$ from the cathode and Zn plating/stripping on the anode during the reversible discharge/charge process. The concern is that cathodes experience substantial volume variations as a result of the larger radius of the Zn $^{2+}$ (74 pm) than Li $^{+}$ (68 pm) [16,17]. This discrepancy often results in the pronounced deterioration of the structure's integrity and the limited utilization of active materials, especially for long cycles. In addition, repeated cycling can also induce the growth of sharp zinc dendrites penetrating separators, resulting in short circuits [18–20], thus

deteriorating the cycle performance of cells. Therefore, the rational design and construction of advanced nanomaterials with high conductivity, fast reaction kinetics, tailororable porous skeletons, and more active sites have become increasingly important as electrode materials for ZIBs have become crucial strategies to address the aforementioned issues [21,22].

Compared to conventional bulk electrodes, nanostructured electrode materials can provide large electrochemical active sites and reduce the ion diffusion path [23], which significantly improves the redox reaction rates and achieves faster kinetics. Among these nanostructured electrodes with different dimensions, for example, vanadium- and manganese-based compounds [24–28], heteroatom-rich organic materials [29–31], porous metal–organic frameworks (MOFs) [32–34], etc., one-dimensional (1D) nanomaterials exhibit numerous advantageous characteristics, including a high surface area, exceptional mechanical strength, and flexibility [35]. These attributes position them as outstanding electrode materials. For example, the rod-like $\text{Na}_{0.95}\text{MnO}_2$, $\text{H}_2\text{V}_3\text{O}_8$ nanowires, and $\text{Zn}_3\text{V}_2\text{O}_8 \cdot 1.85\text{H}_2\text{O}$ nanobelts [36–38] were reported to serve as excellent cathode materials for ZIBs. In addition, 1D nanomaterials can adapt to volume changes and afford interconnected ion/electron pathways, thus boosting the rate capability and cycling stability [39].

Various methods have been reported to fabricate 1D nanomaterials, including pyrolysis, chemical vapor deposition, solution precipitation, and electrospinning [40–42]. Compared to other methods, electrospinning is the most attractive due to its cost effectiveness, controllability, and adaptability in producing functional nanofibers with high conductivity, large surface areas, and porosity. By adjusting the polymer solution and electrospinning parameters, electrospun nanofibers with solid, hollow, porous multichannel and core/shell structures have been successfully prepared and applied in energy storage systems (LIBs [43,44], sodium-ion batteries [45], zinc-air batteries [46], and supercapacitors [47,48]), including electrode materials, nanofiber separators, and gel electrolytes [49]. Similar concepts have also been successfully transferred from other energy storage systems to ZIBs and great achievement has been made in recent years. Although many reviews have summarized the application of electrospun materials in different kinds of electrochemical energy storage systems, most of them are focused on lithium-based or sodium-based energy storage systems; a comprehensive review on ZIBs is still absent. Given the growing interest and rapid progress of electrospinning technology in ZIBs, there is an urgent need to summarize the recent advancements in a timely and systematic manner and provide potential guidelines for the development of high-efficiency ZIBs based on electrospinning.

In this review, recent advances in the design of 1D nanomaterials via electrospinning technology for ZIBs, including cathodes and zinc anodes, are systematically summarized. The electrochemical performance and fabrication strategies of electrospun cathode materials for vanadium-based compounds, manganese-based compounds, organic compounds, and MOF-derived materials are discussed in detail. The modification of zinc anodes, including functional interlayers and functional substrates, is outlined. The summary of electrospun nanostructured materials for ZIBs is shown in Figure 1. We sincerely hope that this review can stimulate researchers' interest in electrospun nanomaterials for ZIBs and promote their practical applications in the future.

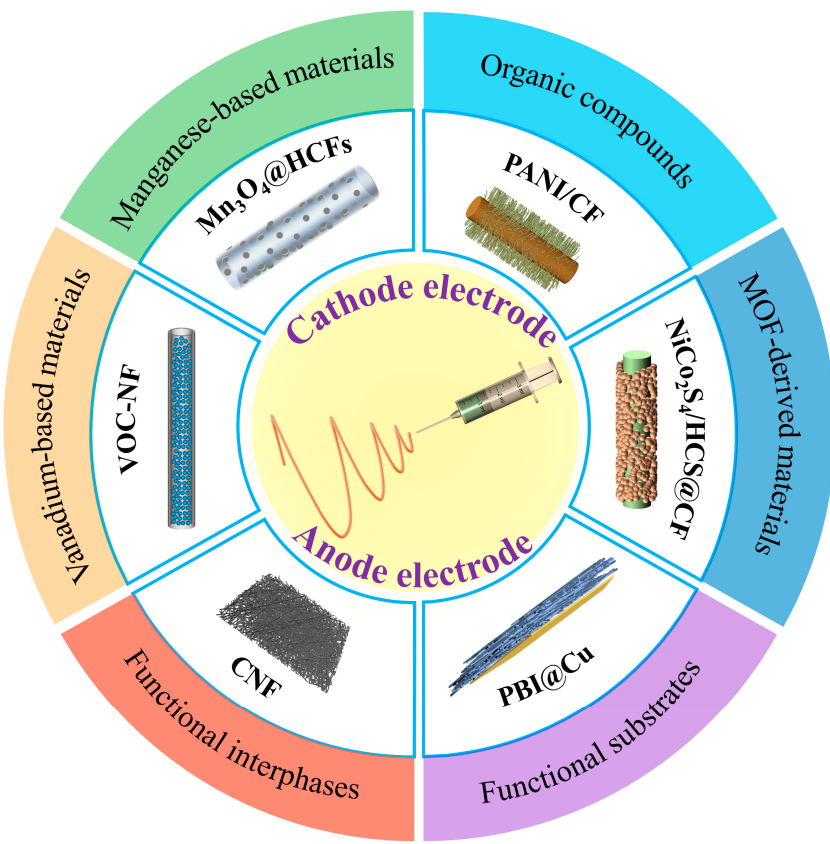


Figure 1. Schematic illustration of electrospun nanostructured materials in ZIBs and representative structural characterization.

2. Electrospinning Technology

2.1. Electrospinning Principle

Electrospinning is used in many different areas as a straightforward, rapid, facile, and scalable strategy for producing ultra-thin fibers [50–52]. As shown in Figure 2a, the typical experimental setup for electrospinning consists of three parts. The first component comprises a high-voltage power supply that can provide $100\text{--}3000\text{ kV m}^{-1}$ between the needle tip and the collector, generating free charges. The second component comprises a syringe pump responsible for regulating the flow of the precursor solution. The third part is a collector (normally a metal film, drum, or mesh) [40]. In general, during the electrospinning process, a viscoelastic precursor solution is added to the syringe and continuously forms a few droplets at the needle tip via a syringe pump. Upon applying a static DC voltage, the interplay of the electrostatic repulsion force, surface tension, and gravity induces the hanging droplet to elongate into a conical shape, commonly named the “Taylor cone” [53]. As the surface charge of the droplet increases, the electrostatic repulsive force breaks through the surface tension, causing the precursor solution to be ejected from the needle tip, forming a liquid jet. The electrostatic repulsive force further stretches the liquid spray into finer diameters and deposits irregularly on the collector. Finally, the ultra-thin nanofibers can be obtained after instantaneous evaporation and solidification of the solvent.

2.2. Factors and Parameters

In general, in an experimental preparation process, it is essential to tune the desired morphologies and structures of the fibers by controlling the internal factors of the precursor solution and the external operating parameters. Usually, the fibers’ diameter and continuity can be regulated by the viscosity of the precursor solution and voltage. A low viscosity and voltage may produce particles but not fibers, while a high viscosity may cause an unstable

solution flow rate. The concentration of the precursor solution is another crucial internal factor. Optimal concentration is often a variable parameter that can be manipulated to achieve fibers with consistent diameters. A lower concentration might lead to insufficient surface tension to counteract the electric field force, causing unraveled fibers. Thus, by controlling the processing parameters, different morphologies and diameters of polymer materials can be obtained, such as micro- and nanofibers and nanoparticles. Adequate conductivity is also necessary to accumulate sufficient charge in the electric field. Solutions with low electrical conductivity will result in the formation of uneven nanofibers. Conversely, excessive conductivity can result in irregular diameters or the formation of ribbon-like fibers. In addition, various 1D nanostructures with different morphologies, structures, and functions can be easily prepared by mixing different types of components, as shown in Figure 2b.

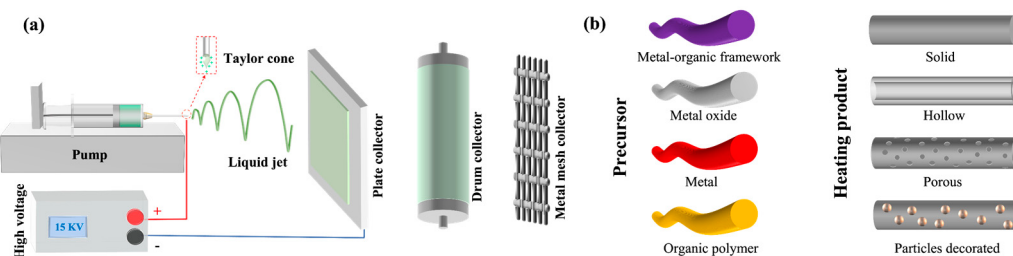


Figure 2. Schematic configuration of (a) the typical electrospinning equipment and (b) the electrospun nanostructures of precursor and calcination products.

The operating parameters of electrospinning include the electric field intensity (E), the flow rate (Q), the electric current (I), and the distance between the needle tip and the collector (D). For example, a higher electric potential will increase the acceleration of the jet, resulting in smaller-diameter fibers. In contrast, a lower voltage will produce thicker-diameter fibers or beaded fibers. The feed rate is a critical parameter in maintaining the formation of nanofibers. A heightened feed rate can result in fibers with spindly beads, whereas a diminished feed rate may lead to fibers with reduced diameters. The distance can be modified to regulate the diameter. Increasing the distance will reduce the diameter of the fibers. It is crucial to emphasize that environmental factors, including humidity and temperature, can influence the formation of fibers. It is therefore important to take these factors into account during the preparation process and not to overlook their effects.

2.3. Collection Devices

The collector functions as a conductive substrate on which the nanofibers are amassed. The nature of the collector can impart varying effects on the resulting nanofibers. In general, the most common collector is the aluminum flat plate, similar to the metal mesh, but other collectors, such as rotating collectors, are also under investigation due to the requirement for aligned fibers in many applications. The rotating collector can adjust its rotational speed to control the degree of fiber alignment. With the increase in rotation speed, the fibers exhibit pronounced alignment along the axis of rotation. Nevertheless, the rotating collector can only partially achieve fiber alignment, as there are still a few fibers with randomly distributed diameters. Another method involves the use of two parallel metal strips spaced a certain distance apart, which can be used as a substrate to create perpendicular fibers that are stretched and aligned by changing the electric field force [54].

2.4. Thermal Treatment

The resulting nanofibers can be further treated by pyrolysis to achieve different properties. In general, the formation of target carbon nanofibers consists of oxidation stabilization and carbonization. Stabilization is necessary to prevent the precursor fibers from melting during the carbonization process. The thermoplastic precursor nanofibers undergo a series of chemical and physical reactions and are finally converted into highly densified thermoset

fibers during stabilization [55]. In addition, the stabilization process involves a relatively slow heating rate to avoid the risk of orientation loss and polymer melting caused by high heat levels. Carbonization involves the transformation from a trapezoidal structure to a graphite-like system, accompanied by cross-linking and reorganization in an inert atmosphere [56]. Different porous structures can be obtained from the release of different gaseous species during the heating process, such as H_2O , H_2 , HCN , N_2 , NH_3 , CO , and CO_2 . Furthermore, during carbonization, the fibers shrink and become much thinner than the precursor fibers, significantly increasing the specific surface area. Finally, these as-prepared carbon nanofibers loaded with active materials can be used as high-performance electrodes in ZIBs.

3. Electrospun Cathode Materials

Cathode materials are critical for ZIBs because they can provide Zn storage sites, influencing the final operating voltage and specific power density. To date, vanadium- and manganese-based materials, Prussian blue analogs (PBAs), organic compounds, metal-organic frameworks (MOFs) [34], and other types of materials have been designed and applied as cathodes in ZIBs. Owing to the multiple valence states, high redox potential, and theoretical capacity, vanadium- and manganese-based compounds are particularly outstanding cathodes for ZIBs. Unfortunately, most of these materials have poor conductivity and dissolution problems during the charge/discharge process, which remain major obstacles to meeting commercial requirements. An effective method of addressing these issues is to integrate carbon materials to form a hybrid nanostructure. Carbon nanomaterials produced by the electrospinning technique can provide cathode materials with high conductivity and serve as matrices with large exposed specific surface areas for embedding nanostructured active materials, which can facilitate fast electrochemical kinetics and inhibit dissolution. In addition, some electrospun composites can be directly used as freestanding and flexible electrodes to construct high-energy-density and flexible ZIBs. The following content summarizes and discusses the recent progress in cathode electrodes achieved by electrospinning methods for ZIBs, including the types of materials, challenges, and viable solutions.

3.1. Vanadium-Based Materials

Vanadium is naturally abundant and has many valence states. As a result, there are many different types of V-based compounds. Among them, V-based oxides have been widely reported, especially V_2O_5 and VO_2 [57–61]. The layered structure of V_2O_5 provides suitable layer spacing for ion migration, and the two-electron transfer reactions of vanadium give it a high theoretical capacity (589 mAh g^{-1}). Unfortunately, the Zn insertion/extraction process is often hindered by poor conductivity and structural instability, causing sluggish kinetics and reduced capacity. Numerous efforts have been made to address these challenges, including combination with conductive materials, crystal structure adjustment, morphology engineering, and other modification strategies [62–65]. It is worth noting that the utilization of 3D networked carbon nanofibers in combination with electrospinning to produce composite materials has become increasingly attractive. For example, Chen's group [66] produced a V_2O_5 carbon fiber cloth (V_2O_5 -CFC) via electrospinning and high-temperature calcination methods, as illustrated in Figure 3a. The V_2O_5 nanosheets are embedded in the ultra-long 1D carbon nanofibers, forming a 3D conductive network structure (Figure 3b). Compared to pure V_2O_5 , V_2O_5 -CFC has a significantly higher cycling stability because of the prevented aggregation of V_2O_5 nanosheets. Wang et al. [67] prepared a V_2O_5 encapsulated core–shell hierarchical structured fiber. The hierarchical organization of the core–shell structure provides a substantial surface area that promotes electron/ion transport. Consequently, it demonstrates excellent rate capability by maintaining an outstanding capacity of 409 mAh g^{-1} even under a high current of 8 A g^{-1} .

In order to optimize the electrochemical performance of V_2O_5 , Chen's group [68] designed porous vanadium oxide fibers (VCN) with abundant defects by electrospinning

and carbonization. Both the physical defects of pore pathways and caverns (Figure 3c) and the chemical defects of oxygen vacancies (Figure 3d) can be concurrently generated during the carbonization process. The defects in the cathodes enhance the ion/electron migration, resulting in a shortened pathway and improved electrolyte penetration. This leads to a remarkable electrochemical performance of the cathodes, achieving a capacity of 256 mAh g^{-1} at 1 A g^{-1} . In addition, Chen's group [69] also demonstrated a type of V_2O_5 nanofiber with a rich mesoporous structure (Figure 3e). This open and stable architecture with rich porosity is beneficial for electrolyte permeation and Zn^{2+} insertion, enabling high reversible capacity with ideal retention after 500 cycles.

Except for the combination of electrospun carbon fibers with excellent conductivity to enhance the conductivity and flexibility of the whole cathode, some work has demonstrated that electrospun polyacrylonitrile (PAN) fibers can be used as a sacrificial template to design one-dimensional V_2O_5 nanostructured materials with interface defects. Due to the high surface area and abundant electroactive sites, these materials are expected to display excellent electrochemical performance. For example, Yoo et al. [70] used a template method to synthesize interface-deficient V_2O_5 nanochips as cathodes (Figure 3f). In the synthesis process, graphene is used to wrap PAN fiber templates embedded with vanadium salt. During annealing, the combusted graphene can induce interfacial oxygen vacancies formed in the V_2O_5 . With the growth of V_2O_5 nanochips, these vacancies were activated by compressive strain, serving as open channels for Zn^{2+} storage. In addition, Yoo et al. [71] also prepared Fe-doped V_2O_5 nanorods by impregnating electrospun PAN fiber templates in the precursor solution (Figure 3g). The doping effect and unique nanorod structure enhance the electrical conductivity and ion migration kinetics, delivering superb rate and cycling capabilities.

Unlike V_2O_5 , which has a narrow interlayer spacing resulting in severe structural degradation during the Zn^{2+} insertion/extraction process, VO_2 has been shown to transform the initial phase into hydrated vanadium oxide ($\text{V}_2\text{O}_5 \cdot n\text{H}_2\text{O}$) through electrochemically induced phase transitions, and the structural H_2O can increase interlayer spacing and reduce electrostatic interactions, thereby effectively enhancing Zn^{2+} diffusion and ensuring structural stability [72]. Thus, Wei's group [73] utilized the *in situ* self-transformation of VO_2 and the electrospinning technique to prepare a kind of self-supported cathode. The binder-free cathode delivers an excellent specific capacity of 319 mAh g^{-1} at 0.1 A g^{-1} and 215 mAh g^{-1} at 20 A g^{-1} (Figure 3h), confirming its significant promise in zinc-ion batteries.

Apart from V_2O_5 and VO_2 , low-valence vanadium oxide V_2O_3 can also be used as a potential V-based cathode for ZIBs owing to its tunnel-like 3D architecture, which can enhance the ion insertion/extraction and reduce the electrical resistance. Recently, Liu et al. [74] reported a nanostructured V_2O_3 /carbon cathode with V_2O_3 nanoparticles embedded in carbon fibers. The electrospun V_2O_3 /carbon composite, with its distinctive tunnel-like 3D structure of V_2O_3 and high electrical conductivity of carbon nanofibers, offers enhanced rate capacity and cycle stability as a flexible and free-standing electrode for ZIBs.

Unlike vanadium oxides, vanadium chalcogenides are also worthy of exploring for their superior electrical conductivity and capacity [75,76]. However, vanadium chalcogenides always suffer from severe dissolution problems during the Zn^{2+} insertion/extraction process, causing structural instability. To overcome this problem, Yang et al. [77] used electrospinning to prepare a flexible cathode film, which allowed for better deposition of the active materials and Al_2O_3 coating layers. These Al_2O_3 nanolayers can not only act as a physical barrier to separate the active material from the electrolyte to prevent the dissolution of VSe_2 but also serve as ion-conducting nanoglue to anchor VSe_2 onto N-CNFs substrates and maintain the structural integrity of the electrodes (Figure 4a). As shown in Figure 4b, TEM confirms that the Al_2O_3 nanocoating layer is homogeneously deposited on the surface of the VSe_2 NSs. The assembled ZIB provides an excellent stack energy density of $\sim 125 \text{ Wh kg}^{-1}$ (Figure 4c).

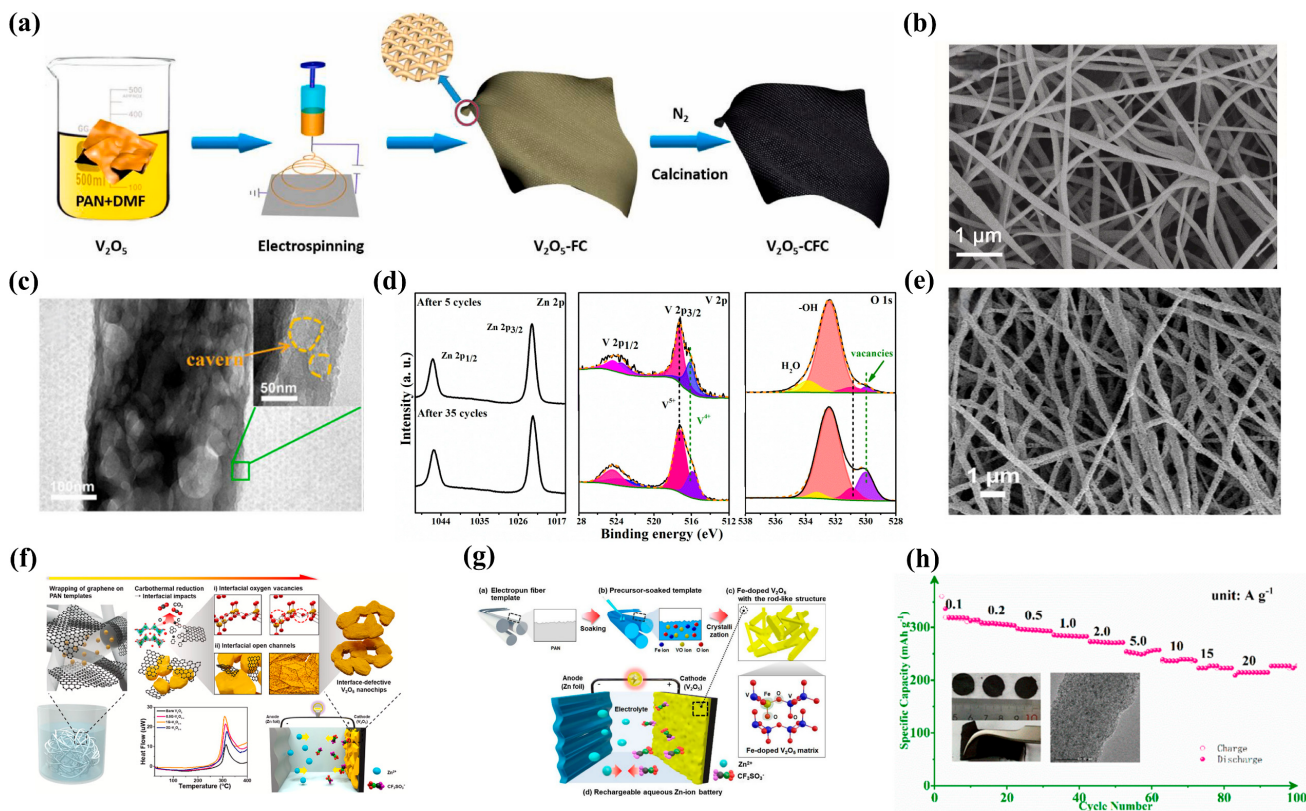


Figure 3. (a) Preparation of flexible V_2O_5 -CFC cathode; (b) SEM image of V_2O_5 -CFC; (c) TEM image of VCN fibers; (d) comparison of XPS spectra of Zn 2p, V 2p, and O 1s regions between the initial and subsequent cycle; (e) SEM image of as-fabricated V_2O_5 nanofibers; (f) schematic of the electrospun PAN templates for the synthesis of interface-defective V_2O_5 nanochips; (g) schematic of the rod-like structure of Fe-doped V_2O_5 synthesized by electrospinning templates; (h) rate capability of VO_2 (insets are photograph of the self-supporting and flexible electrode and the TEM image of the as-prepared nanofibers). (a,b) Reproduced with permission from [66], copyright 2022, Elsevier Ltd. (c,d) Reproduced with permission from [68], copyright 2020, Elsevier Ltd. (e) Reproduced with permission from [69], copyright 2019, Elsevier Ltd. (f) Reproduced with permission from [70], copyright 2021, Elsevier Ltd. (g) Reproduced with permission from [71], copyright 2021, Elsevier Ltd. (h) Reproduced with permission from [73], copyright 2022, American Chemical Society.

Gradient materials have attracted considerable interest due to their compositional distributions, which offer excellent adaptability to specific environmental conditions. However, the production of continuous materials is challenging due to the difficulty of precisely controlling the continuous gradient distribution in their composition and structure. To overcome this obstacle, Hu et al. [78] reported a novel strategy to fabricate continuous gradient composite films (GCFs) by regulating the dynamically changing concentration during electrospinning techniques. The precursor concentration, which decreases from bottom to top, is achieved by continuously adding electrospinning polymer solution to the precursor solution (Figure 4d). VO nanoparticles are consistently distributed within the carbon fiber matrix with gradually decreased concentration from the bottom to the top (Figure 4e). When VO-GCFs were employed as ZIBs cathodes, they displayed outstanding electrochemical performance, and the capacity can still be maintained at 477.1 mAh g^{-1} at a high current of 5.0 A g^{-1} .

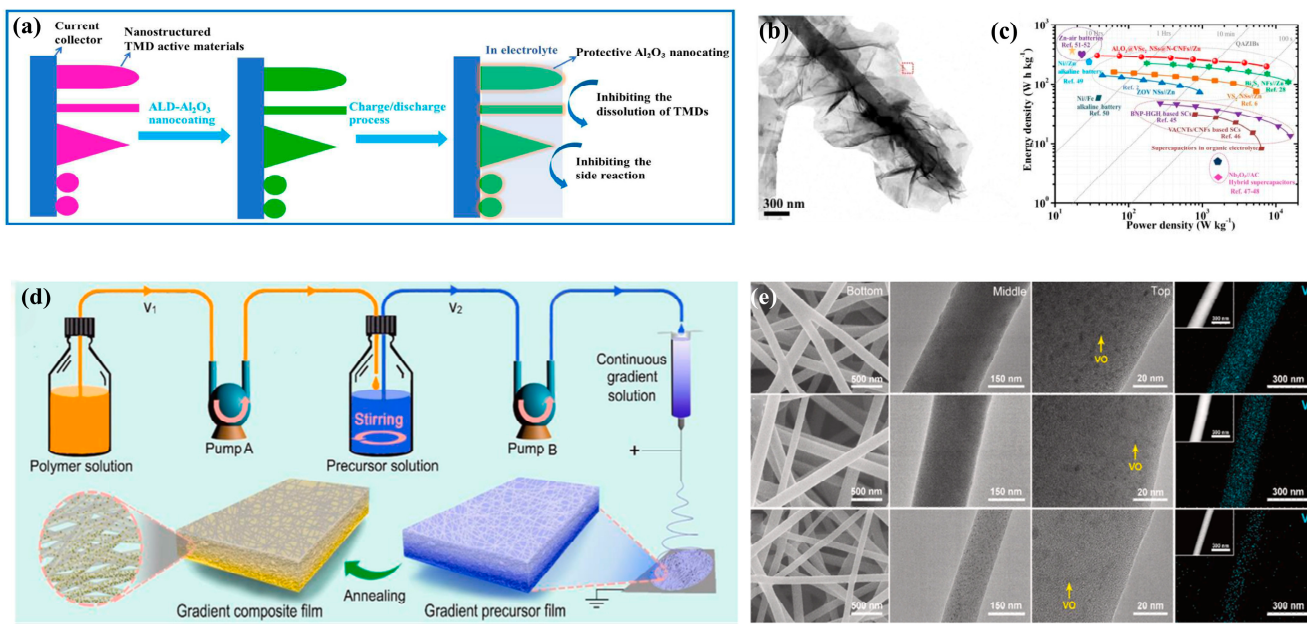


Figure 4. (a) Schematic of introducing protective Al₂O₃ coating layers; (b) TEM image of the Al₂O₃@VSe₂ NSs@N-CNF; (c) Ragone plot comparison with some reported ZIBs; (d) schematic illustration of fabricating GCFs; (e) SEM, TEM, and TEM elemental mapping images of composite nanofibers from left to right. (a–c) Reproduced with permission from [77], copyright 2022, Elsevier Ltd. (d,e) Reproduced with permission from [78], copyright 2022, Elsevier Ltd.

3.2. Manganese-Based Materials

Due to the advantages of being inexpensive, abundant, environmentally friendly, and non-toxic, manganese(Mn)-based oxides with different valence states, such as MnO₂, Mn₂O₃, Mn₂O₄, and Mn₃O₄ [79–82], have been developed as promising ZIBs cathodes. Although Mn-based oxides possess high operating potential, specific capacity, and energy density when used as cathodes for ZIBs, Mn oxides generally suffer from inferior rate performance and cycle stability due to the low inherent electronic conductivity, significant structural damage, and inevitable dissolution of Mn²⁺. An effective approach to tackle these issues involves the integration of nanostructured Mn oxides with conductive substrates. On the one hand, these conductive substrates including carbon cloth and carbon nanofibers can improve the conductivity of the composite. On the other hand, these conductive substrates usually have a high surface area and abundant functional groups, which can prevent the dissolution of Mn²⁺ by adsorption. For instance, Liu's group [83] used a porous carbon fiber (PCF)-loaded MnO₂ (PCF@MnO₂) as a cathode electrode for ZIBs. The PCF mats were synthesized by the initial electrospinning, separation, and subsequent pyrolysis. It shows that mesopores are uniformly distributed in the fiber (Figure 5a) and that thin layers of MnO₂ are uniformly deposited on the internal and external surfaces of the PCF after subsequent incubation in KMnO₄ solutions (Figure 5b). The internal homogeneous mesopores of PCF offer a large surface area and facilitate high MnO₂ loading, and the PCF@MnO₂ with areal MnO₂ loadings of 1.00 and 1.42 mg cm⁻² exhibits superior energy and power densities than other reported cathodes (Figure 5c). Similarly, Fang et al. [84] prepared nitrogen-doped carbon nanofibers (CNFs) by electrospinning polyamic acid (PAA)/polyvinyl pyrrolidone (PVP). Subsequently, ultra-thin MnO₂ nanosheets were in situ grown on the surface of CNFs (Figure 5d). When a Zn(ClO₄)₂ salt is employed for the Zn//MnO₂-CNF ZIBs, the cell exhibits an exceptional cycle life of 500 cycles at 1 A g⁻¹ under 0 °C (Figure 5e) and could light up the LED at an ambient temperature of –10 °C.

The modification of the Mn oxides themselves, such as the creation of heterointerfaces, defect engineering, and pre-intercalation of cations, can be efficient strategies to tune the electronic and crystal structure of the electrode materials, thereby improving the

conductivity and reaction kinetics of Mn oxide-based cathodes. To further enhance the electrochemical behavior of Mn-based oxides, Tang et al. [85,86] developed a heterostructured MnS/MnO composite that has rich heterointerfaces with abundant reaction active sites and N-doping, which significantly improves the electronic conductivity and surface reaction kinetics. In addition, Yang's group [87] reported a novel composite with MnO_2 grown on the carbon nanofibers synthesized by electrospinning as the electrode, due to the interlayer spacing of MnO_2 , was enlarged by the K^+ -intercalation; the resulting materials can maintain a high reversible capacity of 190 mAh g^{-1} at 3 A g^{-1} over 1000 cycles.

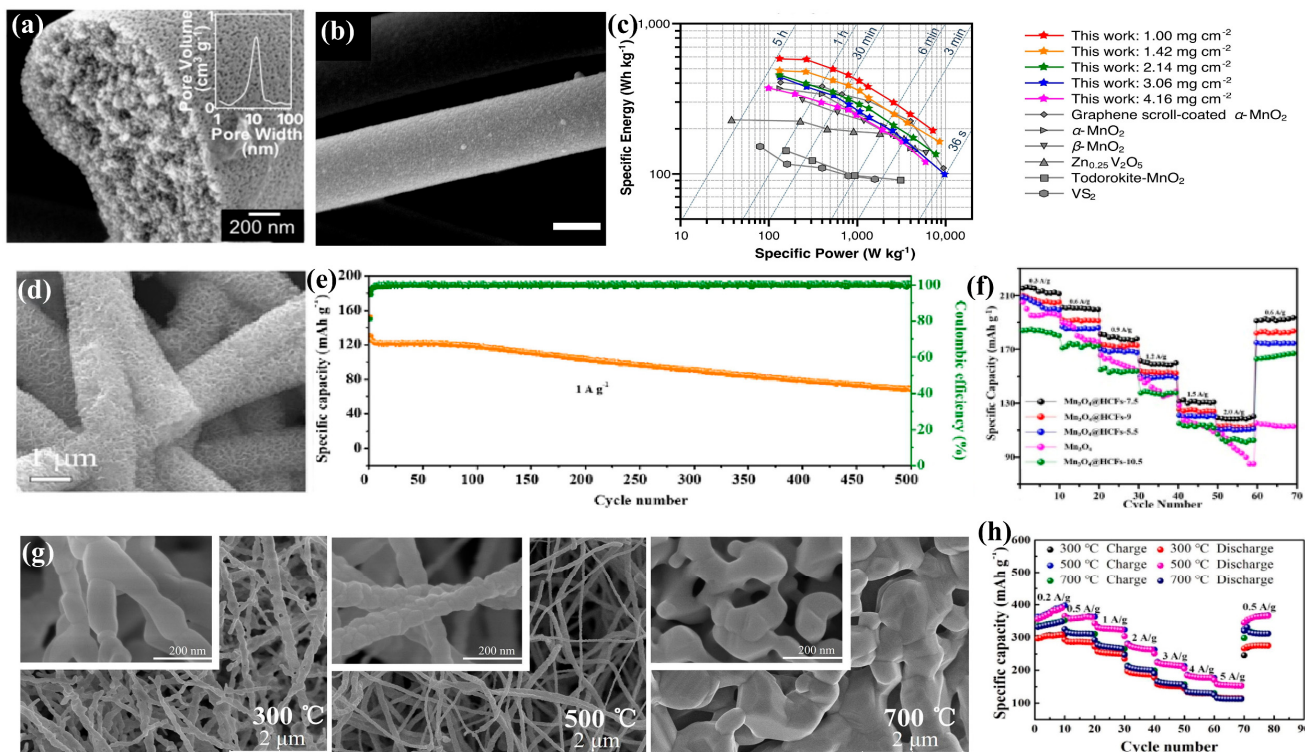


Figure 5. (a) SEM image of PCF; (b) SEM image of PCF@ MnO_2 prepared by solution soaking; (c) comparison of the Ragone plot of PCF@ MnO_2 with other cathodes; SEM images of the (d) MnO_2 -CNFs; (e) the cycling stability of the cell tested at 0°C ; (f) rate performance of all the Mn_3O_4 @HCFs electrodes at different currents; (g) SEM images of different MnO_x nanowires annealed at 300°C , 500°C , and 700°C ; (h) rate performance of different MnO_x nanowires annealed at 300°C , 500°C , and 700°C . (a-c) Reproduced with permission from [83], copyright 2022, Wiley-VCH Verlag GmbH & Co. KGaA, Weinheim. (d,e) Reproduced with permission from [84], copyright 2023, Elsevier Ltd. (f) Reproduced with permission from [88], copyright 2020, Elsevier Ltd. (g,h) Reproduced with permission from [89], copyright 2022, Elsevier Ltd.

To further investigate the effect of the carbonization process, including carbon content and carbonization temperature, on the electrochemical behavior of the 3D carbon network composited with Mn-based materials, Long et al. [88] investigated the effect of carbon content in the Mn-based oxides/carbon nanofibers on the electrochemical performance. Different PAN contents (5.5%, 7.5%, 9%, 10.5%) in the spinning solutions were combined with Mn_3O_4 nanoparticles (NPs) to adjust the carbon content. Lower carbon content cannot fully embed all the NPs, resulting in partial aggregation. However, excessive carbon content will reduce the porosity, inhibiting ion transport and electrolyte infiltration. Thus, the well-defined Mn_3O_4 @HCFs-7.5 electrode demonstrates excellent rate capability (215.8 and 115.7 mAh g^{-1} at 0.3 and 2.0 A g^{-1} , respectively, Figure 5f). In addition, Cheng et al. [89] explored the temperature effect on the electrochemical behavior. As depicted in Figure 5g, when treated at 500°C , the Mn_2O_3 nanoparticles were uniformly

embedded in the carbon nanowires, compared to the uneven nanowire formation and discontinuous grain growth at 300 °C and fiber disintegration and bead-like particles at 700 °C. When employed as ZIB cathodes, the Mn₂O₃ obtained at 500 °C shows outstanding rate performance (~153 mAh g⁻¹ at a current of 5 A g⁻¹, Figure 5h).

3.3. Organic Compounds

Organic compounds play an important role as ZIB cathode materials due to their lightweight, renewable resources, environmental friendliness, and structural diversity. In contrast to transition metal oxides, the redox chemistry in organic electrodes involves only the rearrangement of chemical bonds through the insertion/extraction of large hydrated Zn²⁺. This characteristic helps to avoid significant structural changes [90]. Conductive polymers are a distinctive group of organic materials that exhibit high electronic conductivity due to long electron-conjugated systems. However, the specific capacity and cycling stability of conductive polymers are limited at high doping states when used as electrode materials for ZIBs due to the poor conductivity in this state. Thus, hybridization with conductive substrates is an effective way to improve their electrochemical performance. For instance, Kim's group [91] fabricated polyaniline (PANI)-coated carbon fibers (PANI/CFs) and assembled them as cathodes to construct highly customized high-power ZIBs. A binder-free CF mat was first synthesized as a 3D current collector via electrospinning; then, PANI can be polymerized *in situ* on the surface of the CFs to obtain the desired PANI-coated CF cathode (Figure 6a). As displayed in Figure 6b,c, the thin and highly porous PANI layer grows homogeneously over the entire surface of the flexible CF mat. The packaged PANI/CF/Zn cell within 3D printed geometries exhibits a high rate performance (~600 C). Liu et al. [92] synthesized synchronous ultra-high conductivity reactive N-atom-doped flexible carbon nanofiber networks (SH-FCNNs) by electrospinning. PANI-implanted highly porous polyacrylonitrile (PPAN@PANI) nanofibers were used as precursors due to the strong interaction between their functional groups (Figure 6d). Flexible solid-state ZIBs packed with commercially available aluminum plastic films were fabricated, realizing superior rate capability (132 mAh g⁻¹ at 20 A g⁻¹, Figure 6e) and cycle performance (168.2 mAh g⁻¹ after 5000 cycles at 5 A g⁻¹, Figure 6f). Apart from PANI, Cai et al. [93] reported that poly(5-cyanoindole) could be directly electrospun into fibers to serve as cathode materials for ZIBs, giving discharge capacity (107 Ah Kg⁻¹) superior to that of the zinc/polyindole powder cell.

3.4. MOF-Derived Materials

Organic ligands coordinated with metal ions form metal–organic frameworks (MOFs), which are gaining interest as advanced functional electrode materials in battery systems due to their high porosity, large surface area, and controlled morphologies. MOFs can be selected as precursors or templates to be converted into specific carbon-based derivatives to improve their electrical conductivity and structural integrity [94], which enhances electron migration and prevents volume fluctuations. For example, Yu et al. [95] prepared MOF-derived NiCo₂S₄ nanoparticles and hollow carbon hybrid spheres compactly connected by electrospun carbon fibers (NiCo₂S₄/HCS@CFs) and used them as binder-free cathodes for ZIBs (Figure 7a). As shown in Figure 7b,c, the solid NiCo-MOF spheres have a smooth surface, and after carbonization and sulfidation of the electrospun composite, necklace-like NiCo₂S₄/HCS@CF were formed with compactly linked structures. The assembled NiCo₂S₄/HCS@CFs/Zn batteries show an extremely high capacity of 343.1 mAh g⁻¹ at 3.8 A g⁻¹ with superior rate and cycle performance (Figure 7d). Zhang et al. [96] reported a 3D self-supported composite with vanadium nitride wrapped in nitrogen-doped carbon nanofibers by electrospinning and annealing. The X-ray diffraction (XRD) pattern depicted in Figure 7e confirms that the crystalline V-MOFs were completely transformed into VN after thermal treatments. The presence of V-based MOFs can induce the formation of whisker-like secondary structures and uniform distribution of VN nanograins. As displayed in Figure 7f, the VN/N-CNFs possess a rough surface with truck nanofibers

and branched nanowhiskers, which can expose more active sites for Zn^{2+} storage. Due to the high structural integrity of the 3D electrospun VN/N-CNF skeletons, the electrode delivered superior cycle stability, maintaining a capacity of 482 mAh g^{-1} after 30,000 cycles at 50 A g^{-1} (Figure 7g). Ding et al. [97] reported a bead-like manganese oxide embedded in electrospun carbon nanofibers ($\text{MnO}_x\text{-CNFs}$); the unique structure can provide robust structural integrity and accelerate the electron/ion diffusion kinetics. These features made $\text{MnO}_x\text{-CNFs}$ exhibit long cycle stability and superior rate capability.

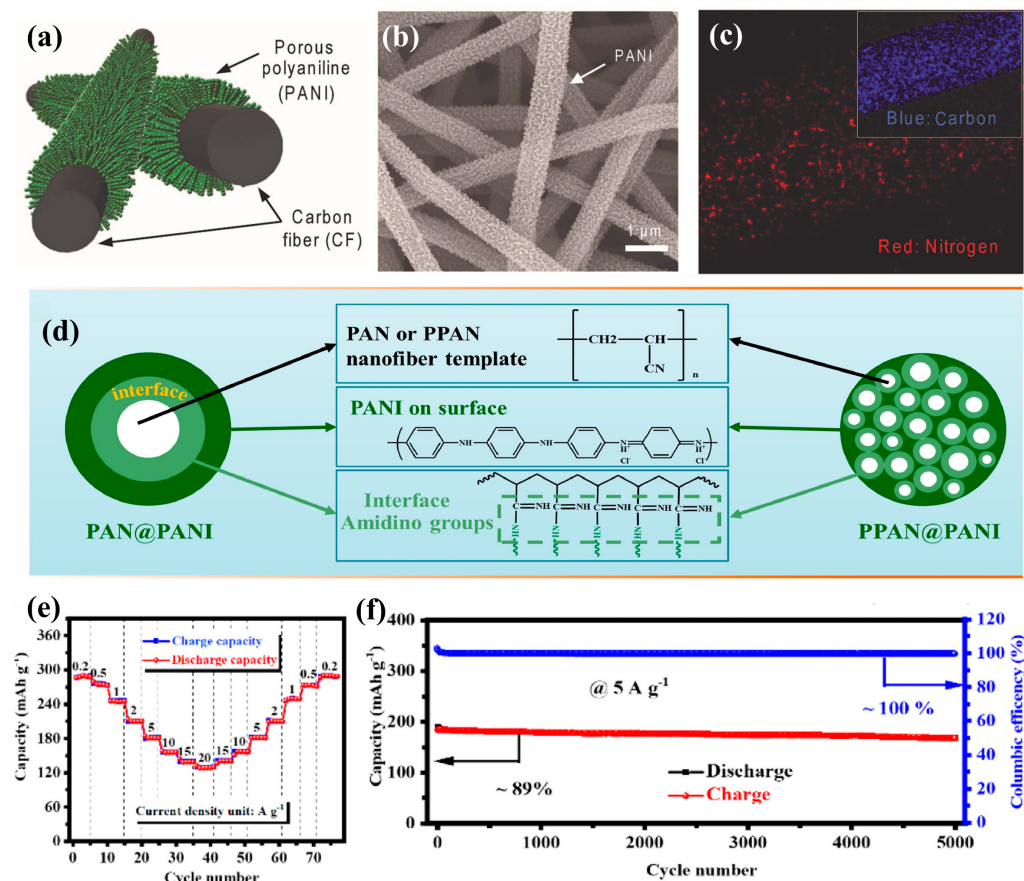


Figure 6. (a) Schematic of the assembly of PANI and CF mat; (b) the SEM image of PANI/CF; (c) elemental maps of a representative PANI/CF cathode; (d) schematic of the interplay between PAN@PANI and PPAN@PANI nanofibers; (e) rate performance and (f) cyclic stability of SH-FCNNs@PANI applied in flexible solid-state ZIB. (a–c) Reproduced with permission from [91], copyright 2018, American Chemical Society. (d–f) Reproduced with permission from [92], copyright 2021, Elsevier Ltd.

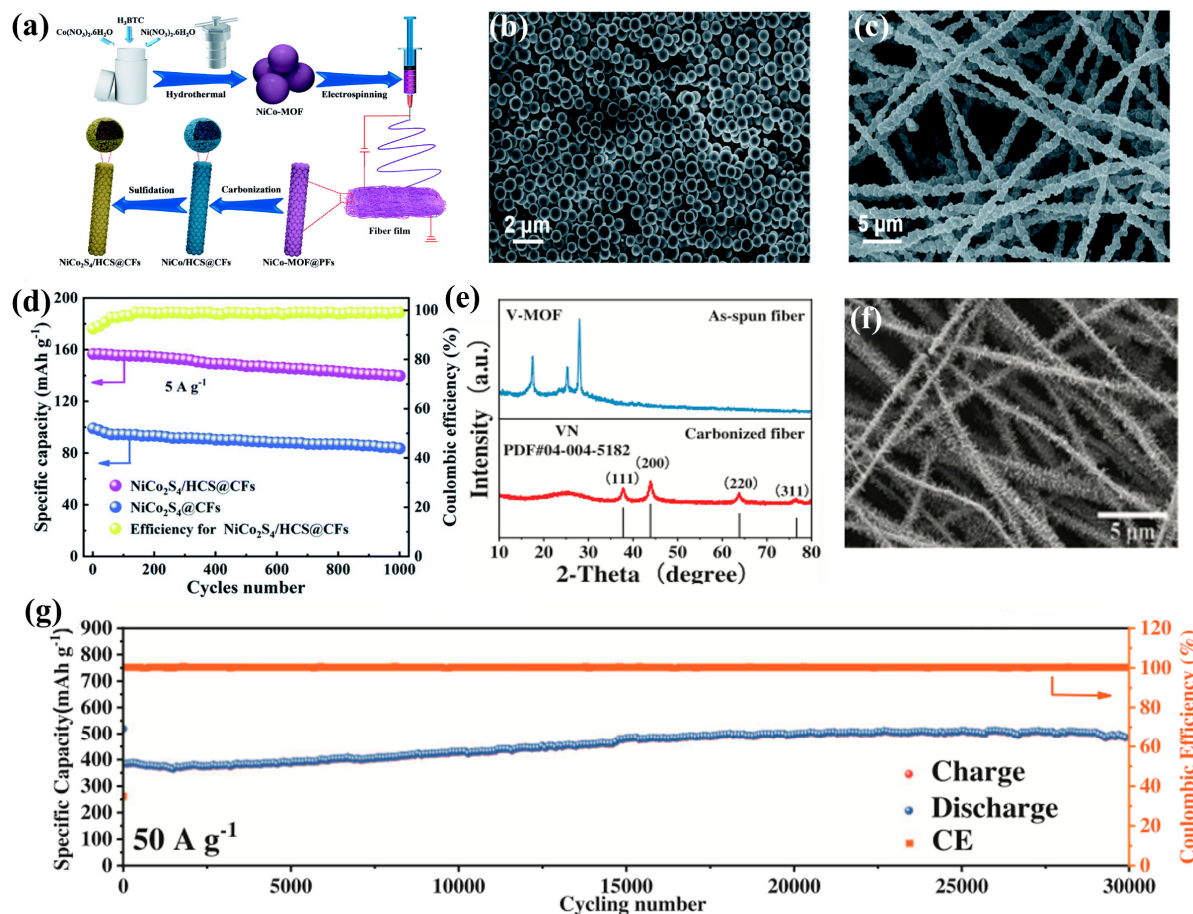


Figure 7. (a) Schematic presentation of the preparation of self-standing $\text{NiCo}_2\text{S}_4/\text{HCS@CF}$ electrode; SEM images of the (b) NiCo-MOF spheres and (c) $\text{NiCo}_2\text{S}_4/\text{HCS@CFs}$; (d) cycling stability of $\text{NiCo}_2\text{S}_4/\text{HCS@CFs}$ and $\text{NiCo}_2\text{S}_4/\text{CF}$ electrodes; (e) XRD patterns of as-spun nanofiber precursor and carbonized product; (f) SEM image of VN/N-CNFs; (g) long-term cycling test at 50 A g^{-1} . (a–d) Reproduced with permission from [95], copyright 2022, Royal Society of Chemistry. (e–g) Reproduced with permission from [96], copyright 2022, Wiley-VCH Verlag GmbH & Co. KGaA, Weinheim.

4. Electrospun Anode Materials

Zinc is commonly used as an anode in ZIBs because of its cost-effectiveness, economical nature, high capacity (820 mAh g^{-1} ; 5851 mAh cm^{-3}), suitable redox potential (-0.76 V vs. standard hydrogen electrode (SHE)), and stability in many environments [98–100]. However, the use of conventional zinc anodes suffers from several issues, including interfacial corrosion, dendrite and “dead zinc” formation during cycling, resulting in problems like poor reversibility, low Coulombic efficiency (CE), and inferior cycle stability, which significantly limit the further practical application of ZIBs. In recent years, many efforts have been made to solve these issues, including electrolyte optimization, hierarchical current collector design, and surface modification [101–103]. Numerous studies have demonstrated that 3D conductive structured materials can act as interfacial layers and substrates, providing abundant zincophilic sites that can alleviate dendrite growth and greatly enhance the rate and stability of ZIBs. Here, the latest advancements in anode electrodes achieved through electrospinning technologies are reviewed. The electrospun modification structure on anodes can be mainly categorized into functional interlayers and functional substrates.

4.1. Functional Interlayers

Many chemical reactions occur on the electrode/electrolyte interface. These reactions include the in situ formation of the solid electrolyte interphase (SEI), ion transport, deposi-

tion, and corrosion of metallic Zn. The interphase on the Zn anode plays a crucial role in determining the thermodynamic stability as well as the dynamic processes that ultimately affect the electrochemical performance of ZIBs. To promote Zn^{2+} migration and induce homogeneous Zn plating, surface modification of the anode with a microporous polymer network or the addition of an interlayer between the separator and the zinc anode is considered a promising strategy. Coincidentally, the electrospun nanofiber membrane, with its lightweight and self-supporting properties, is a good choice as an interlayer material. For example, Kim's group [104] modified the Cu foil with an electrospun porous PAN nanofiber layer and employed it as a current collector for the Zn plating/stripping (Figure 8a). The polar nitrile groups present in the PAN nanofibers facilitate the uniform nucleation of zinc and prevent the growth of dendrites. As shown in Figure 8b, the symmetrical cell test demonstrates that the Zn@PAN-Cu electrode has extended cycling stability without a short circuit happening after approximately 270 h. Kim's group [105] also reported that an electrospun ferroelectric poly(vinylidene fluoride-*co*-trifluoroethylene) copolymer (P(VDF-TrFE)) nanofiber layer, denoted as PNF, can yield homogeneous Zn deposition and inhibit side reactions. In addition, Zhao's group [106] demonstrated that the polybenzimidazole (PBI) nanofibers with abundant N-containing functional groups not only allow uniform Zn nucleation on the Cu surface but also facilitate the uniform transport of Zn^{2+} ions, facilitating the uniform deposition of zinc on the 3D porous framework. After 100 cycles of the symmetrical cell test, it can be clearly seen that the surface of the Zn@PBI-Cu anode was relatively uniform without obvious dendrites and flakes structures (Figure 8c,d) formed. Furthermore, the assembled Zn@PBI-Cu/MnO₂ full battery exhibited an exceptional capacity retention of almost 100% after 1000 cycles (Figure 8e). These results demonstrate that the PBI framework can confine the Zn growth in the porous structure and inhibit the short circuits that occur during the long-term cycling test. The electrospun interwoven membranes have an inherently porous structure, which makes it possible to introduce some fillers into the nanofibers or the porous networks to improve the electrochemical behavior of the ZIBs. For instance, Zhi's group [107] synthesized a hierarchical polymer electrolyte by grafting polyacrylamide (PAM) onto an electrospun PAN network. The hybrid membrane can be used both as a separator and an interlayer, and the fabricated flexible solid-state ZIB delivers superior areal energy density and power density. Liu et al. [108] reported a hybrid interlayer consisting of a thermoplastic polyurethane (TPU) fiber matrix and a Zn-alginate (ZA) filler, denoted as Zn@TPZA. This interlayer acts as a physical barrier between the anode and electrolyte, preventing the spontaneous corrosion and uncontrolled accumulation of Zn dendrites. As depicted in Figure 8f,g, the Zn@TPZA-coated zinc anode retains its original shape after 30 days of immersion in a 2 M ZnSO₄ electrolyte with no by-products detected compared to bare Zn, confirming that the hybrid interlayer has excellent corrosion resistance.

Recently, porous and conductive carbon networks derived from electrospun polymer nanofibers have shown great promise as anode interlayers owing to their high electrical conductivity, significant surface area, and unique anisotropic structure, which can homogenize the charge distribution and reduce the nucleation overpotential and diffusion resistance of Zn^{2+} , thus inhibiting the dendrite growth and improving the cycling stability. For instance, Liang et al. [109] demonstrated a N-O co-doped carbon nanofiber (CNF) with a diameter distributed in the range of 500–800 nm (Figure 8h), which can be easily obtained by calcining PAN nanofibers. Owing to the fact that the CNF interlayer can efficiently capture Zn^{2+} and facilitate proper Zn deposition on the anode, the assembled symmetric cell can operate steadily for 1200 h with a low overpotential of 59.5 mV at 5 mA cm⁻² (Figure 8i). Similarly, Wan et al. [110] synthesized a dendrite-free N-doped carbon nanofiber Zn anode and fabricated a ZIB full cell with an Al_xV₂O₅ cathode; the cell can display an energy density of 50 Wh kg⁻¹. Additionally, Yang et al. [111] fabricated a flexible coating layer composed of Cu nanoparticles and porous and conductive carbon networks (Cu@CNFs) by the electrospinning method. Cu nanoparticles (CuNPs) with zincophilic properties can act as nucleation seeds, promoting uniform zinc deposition and preventing dendrite growth,

while the CNFs have the ability to evenly disperse the electric charge and control the flow of Zn^{2+} ions. This synergistic effect efficiently improves its electrochemical performance, resulting in a continuous cycle of over 2200 h at 1.0 mA cm^{-2} .

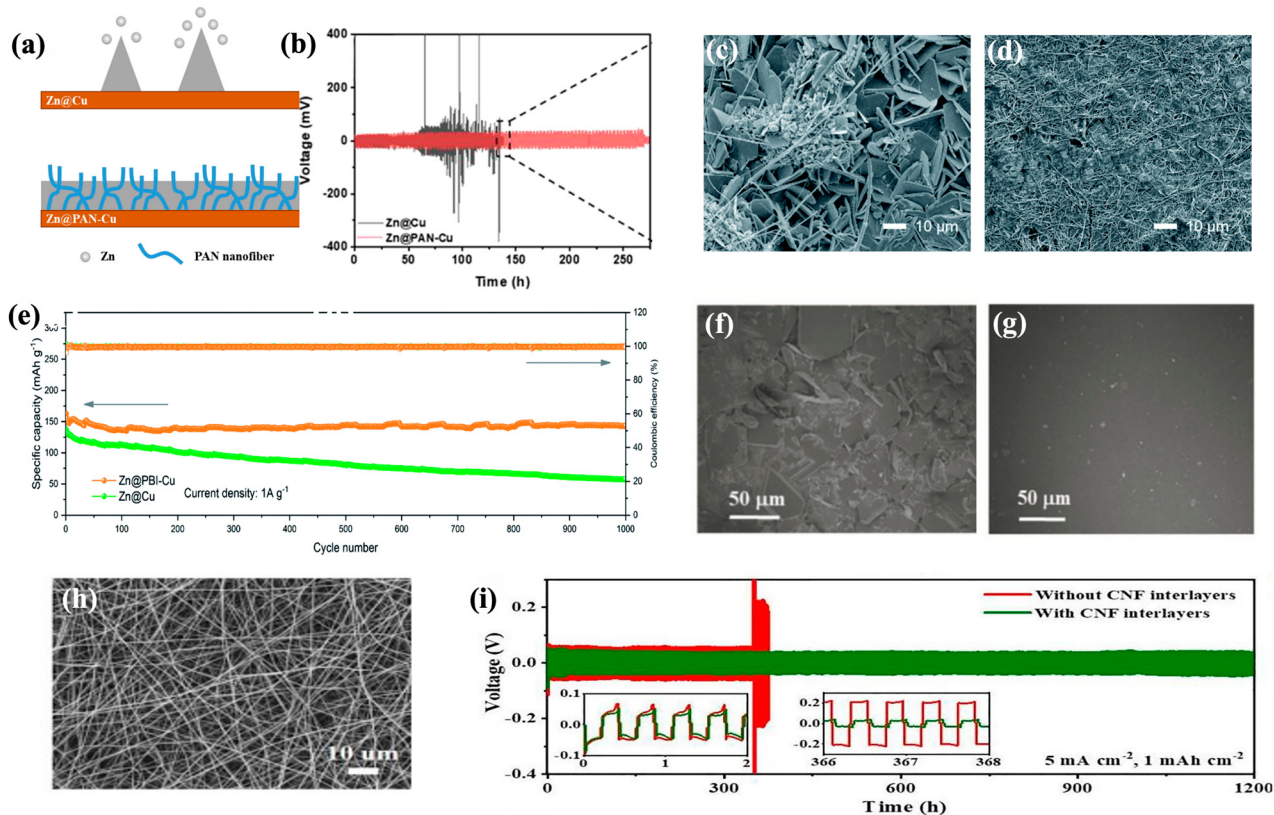


Figure 8. (a) Schematic of the zinc deposition on the Zn@Cu and Zn@PAN-Cu interlayer; (b) symmetrical Zn@Cu and Zn@PAN-Cu cells are tested for cycling performance; SEM images of (c) Zn@Cu and (d) Zn@PBI-Cu after 100 cycles at 10 mA cm^{-2} ; (e) long-term cycling test at 1000 mA g^{-1} of Zn@PBI-Cu/MnO₂ full battery; SEM images of (f) bare Zn and (g) Zn@TPZA electrode after soaking in electrolyte for a few days; (h) SEM image of CNF interlayers; (i) cyclic stability test of Zn deposition/stripping and corresponding nucleation overpotential. (a,b) Reproduced with permission from [104], copyright 2022, Elsevier Ltd. (c–e) Reproduced with permission from [106], copyright 2020, Royal Society of Chemistry. (f,g) Reproduced with permission from [108], copyright 2022, Wiley-VCH Verlag GmbH & Co. KGaA, Weinheim. (h,i) Reproduced with permission from [109], copyright 2021, Elsevier Ltd.

4.2. Functional Substrates

When Zn foils are used directly as the current collector and anode material in ZIBs, their electrochemical properties become unstable due to the volume change and the formation of uneven zinc dendrites during cycling. Apart from the modification of the Zn anode with an interlayer, in recent years, it has also been essential to construct suitable substrates as hosts for the Zn deposition, which can handle the volume change, regulate the crystal orientation, and improve the stability of the Zn anode. CNFs can be regarded as an excellent modification material for conductive substrates due to their high electrical conductivity, large surface area, and unique anisotropic structure for zinc storage. Baek et al. [112] used the CNF as a conductive host for the anode of ZIBs. The symmetrical cell test at 0.1 mA cm^{-2} for 400 h showed that the overpotential of zinc-deposited CNF (ZnCNF) was maintained at 60.1%, which is lower than that of bare zinc. In addition to using conductive materials alone as substrates, another effective approach is to combine 3D conductive frameworks and active materials with abundant zincophilic sites. On the one hand, the 3D conductive frameworks can provide more space than a planar configuration, which is

beneficial in regulating the local current distribution and accommodating the volumetric changes. On the other hand, the use of these active materials significantly regulates the crystal orientation and deposition behavior of metallic zinc, resulting in a notable enhancement in its electrochemical behavior. For example, Yang et al. [113] fabricated a Sn-coated porous carbon fiber (Sn-PCF) as a Zn anode host to promote homogeneous Zn plating. The Sn-PCF@Zn anode synergistically integrates the benefits of two constituent elements. One originates from the PCF network, which facilitates the promotion of consistent Zn^{2+} flow and even distribution of 3D Zn formation. The other originates from the Sn nanodot coating, which creates a surface on each fiber that strongly attracts zinc ions and allows for high Zn^{2+} adsorption and immobilization. These features work together to enhance the Zn deposition and stripping behavior, resulting in a very slow capacity degradation rate of approximately 0.009% per cycle at 5 A g^{-1} for Zn-ion full cells. Similarly, Yu et al. [114] reported a 3D hybrid fiber substrate consisting of interconnected N-doped hollow carbon spheres embedded with Sn nanoparticles (Sn@NHCF) as a Zn host for a stable Zn anode in ZIBs (Figure 9a). Compared to the direct coating of Sn nanodots on carbon fibers, this synthesis method, in which Sn nanoparticles are first embedded in hollow carbon spheres and then combined with carbon fibers, provides more internal and external surfaces for Zn deposition, resulting in a lower nucleation overpotential (11.4 mV at 1 mA cm^{-2} vs. 21 mV at 1 mA cm^{-2} , Figure 9b). In addition, a full cell assembled with the Sn@NHCF-Zn composite anode and a V_2O_5 cathode exhibits excellent rate performance and long-term cycle life (Figure 9c). Zeng et al. [115] fabricated a 3D multifunctional host comprising N-doped carbon fibers with Cu nanoboxes (Cu NBs@NCFs) implanted for stable Zn anodes. The preparation of Cu NBs@NCFs is demonstrated in Figure 9d, where the CuS hollow nanoboxes are used as the template for Cu NBs (Figure 9e). The Cu NBs@NCF host demonstrates high Zn deposition/stripping CE for 1000 cycles and extended cycle life (450 h) by inhibiting the dendrite formation. The transition metal oxides (e.g., TiO_2 , SiO_2) have been investigated as Li hosts to suppress dendrite growth and exhibit excellent electrochemical performance in lithium batteries [116,117]. To confirm that these metal oxides can also be used as Zn hosts in Zn batteries, Song et al. [118] synthesized a ZnO_x embedded in porous carbon nanofibers ($ZnO_x@PCNF$) as a host material for Zn anodes. As shown in Figure 9f, the flexible $ZnO_x@PCNF$ films offer stable plating/stripping within 500 h at a high current density, demonstrating that this composite can regulate the electron/ion flux and guide the Zn^{2+} ions to form homogeneous Zn metal deposition. Xue et al. [119] synthesized well-distributed TiO_2 , SiO_2 , and carbon into the 3D porous hollow fiber (HSTF) as a superzincophilic zinc anode host. The homogeneous zinc plating behavior in the 3D-HSTF host can be directly observed using atomic force microscopy (AFM) height tests and Kelvin probe force microscopy (KPFM) potential measurements. As depicted in Figure 9g, the initial HSTF electrode exhibits a relatively smooth surface (the average height is only 370 nm) compared to the rough surface (the average height is 420 nm) of the Zn anode based on a pristine separator.

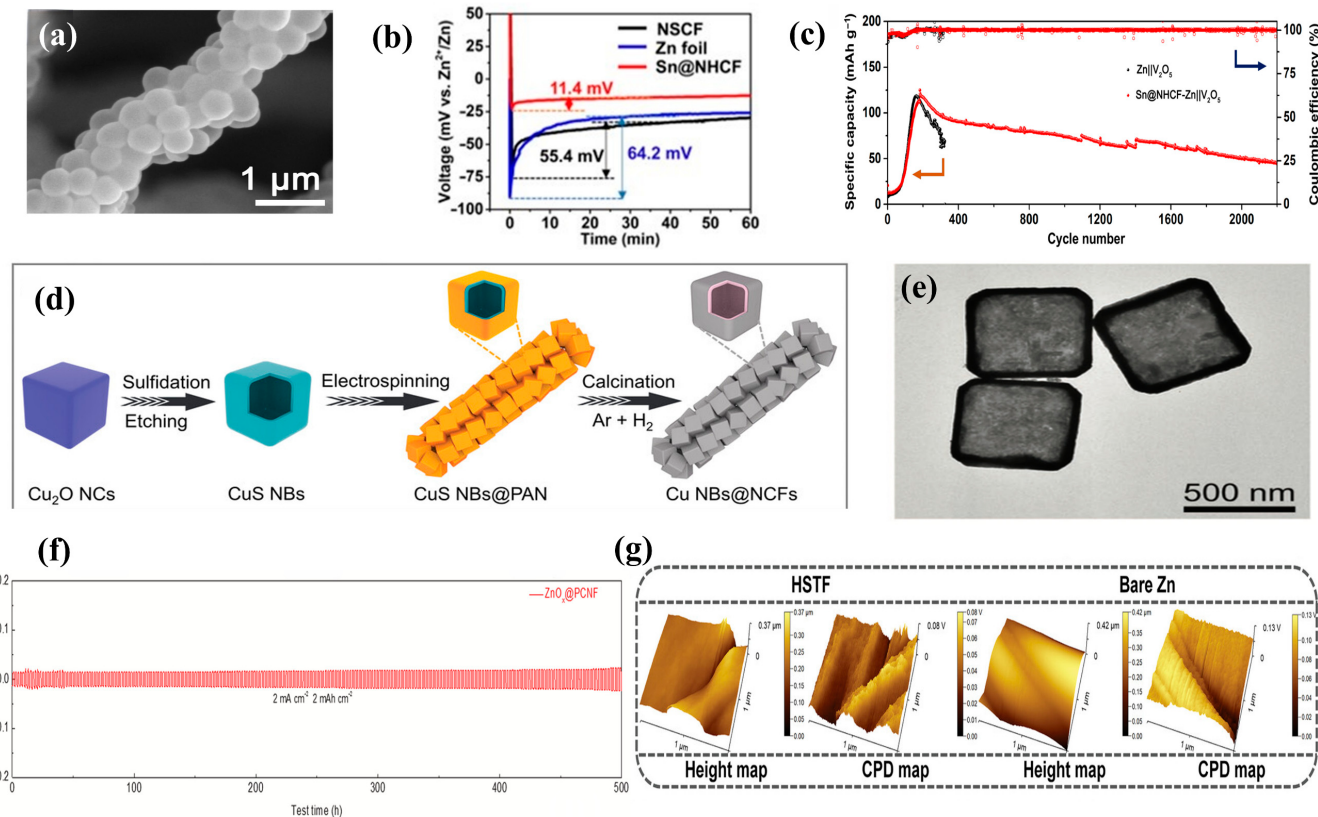


Figure 9. (a) The SEM image of Sn@NHCF; (b) overpotential of Zn deposition on different substrates at 1 mA cm^{-2} ; (c) cycling stability test of the Sn@NHCF-Zn/V₂O₅ and the Zn/V₂O₅; (d) diagram of the preparation process of Cu NBs@NCFs; (e) TEM image of CuS NBs; (f) cycling performance of the ZnO_x@PCNF/Zn/ZnO_x@PCNF/Zn symmetric cells; (g) AFM and KPFM images of the 3D-HSTF and bare Zn. (a–c) Reproduced with permission from [114] Copyright 2019, American Association for the Advancement of Science. (d,e) Reproduced with permission from [115], copyright 2022, Wiley-VCH Verlag GmbH &Co. KGaA, Weinheim. (f) Reproduced with permission from [118], copyright 2021, Elsevier Ltd. (g) Reproduced with permission from [119], copyright 2021, Wiley-VCH Verlag GmbH &Co. KGaA, Weinheim.

5. Conclusions and Perspectives

In recent years, ZIBs have evoked much interest in grid-scale energy storage due to their inherent safety, cost-effectiveness, and environmental friendliness. However, there are still many challenges to be overcome before practical implementation, including extremely unstable Zn metal anodes, side reactions (e.g., H₂/O₂ evolution), cathode dissolution, and structural damage. In this case, numerous efforts have been made to develop and modify the cathode, interlayer, and anode materials in ZIBs. Electrospinning is a highly efficient technology and is widely used to design 1D nanostructures with controllable morphology, structure, and composition by adapting the parameters of electrospinning and annealing. In this review, the basic electrospinning technique has been introduced and its applications in ZIBs have been systematically summarized. For the cathode side, almost all commonly used cathode materials with nanoscale dimensions can be fabricated by electrospinning via modulating the precursor solutions, including vanadium-based compounds, manganese-based compounds, organic compounds, and MOF-derived materials. The 1D nanostructures synthesized by electrospinning can be interwoven to form a 3D network, which improves electrical conductivity and maintains structural integrity. For the anode side, the 3D network interlayers of electrospun polymer nanofibers could homogenize the charge distribution on the zinc anode and promote Zn deposition uniformly, thus inhibiting dendrite formation. In addition, the electrospun carbonaceous nanofibers or composites

have a good surface affinity for Zn^{2+} , thus exhibiting a smoother Zn plating/stripping process, and can construct a CNF/Zn anode by the plating method. However, before designing electrospun nanostructures for ZIBs in future work, there are still several points to consider, including the following: (1) Previous work has mainly focused on the design of transition metal oxide-based cathode materials. Other potential cathode materials, such as organic compounds and MOF-derived composites, are still lacking, and much effort is needed to design these materials with high performance; (2) Innovative strategies based on electrospinning need to be developed to prepare functional components for ZIBs, such as hierarchical separators and solid/gel polymer electrolytes; (3) The testing standards of electrospun nanostructured electrodes need to be established. The loading density, thickness, electrode areas, porosity, etc., of electrospun electrodes are not unified across different reported work, making it difficult to evaluate the effect of different modification strategies, especially for industrial requirements; (4) Currently reported works usually use harmful and flammable organic solvents and expensive precursors, which make it difficult to meet the industrial standard. Thus, the exploration of low-cost precursors and environmentally friendly solvents is urgently needed to promote electrospun nanostructured electrodes for large-scale use. In addition, a reliable and widely applicable mathematical model for optimization of the electrospinning process's parameters also needs to be developed, which can help provide a deeper scientific understanding of electrospinning and promote the development of ZIBs in the near future.

Author Contributions: L.Z. and C.W. contributed equally to this work. Conceptualization, J.C. and S.L.; methodology, C.W., M.-F.L. and A.L.-S.E.; writing—original draft preparation, L.Z.; writing—review and editing, J.C. and S.L.; visualization, C.W. and L.G.; supervision, M.-F.L. and A.L.-S.E. All authors have read and agreed to the published version of the manuscript.

Funding: This research was funded by the National Natural Science Foundation of China (Nos. 52102117, 22175154), China Postdoctoral Science Foundation (No. 2022M712867), and Key Science and Technology Program of Henan Province (No. 202102310212).

Data Availability Statement: Not applicable.

Conflicts of Interest: Author Alice Lee-Sie Eh was employed by the company Metrohm Singapore Pte Ltd. The remaining authors declare that the research was conducted in the absence of any commercial or financial relationships that could be construed as a potential conflict of interest.

References

- Chu, S.; Cui, Y.; Liu, N. The path towards sustainable energy. *Nat. Mater.* **2017**, *16*, 16–22. [[CrossRef](#)] [[PubMed](#)]
- Deng, J.; Lu, X.; Liu, L.; Zhang, L.; Schmidt, O.G. Introducing rolled-up nanotechnology for advanced energy storage devices. *Adv. Energy Mater.* **2016**, *6*, 1600797. [[CrossRef](#)]
- Yang, J.; Yin, B.; Sun, Y.; Pan, H.; Sun, W.; Jia, B.; Zhang, S.; Ma, T. Zinc anode for mild aqueous zinc-ion batteries: Challenges, strategies, and perspectives. *Nano-Micro Lett.* **2022**, *14*, 42. [[CrossRef](#)] [[PubMed](#)]
- Zeng, A.; Chen, W.; Rasmussen, K.D.; Zhu, X.; Lundhaug, M.; Müller, D.B.; Tan, J.; Keiding, J.K.; Liu, L.; Dai, T.; et al. Battery technology and recycling alone will not save the electric mobility transition from future cobalt shortages. *Nat. Commun.* **2022**, *13*, 1341. [[CrossRef](#)] [[PubMed](#)]
- Shen, X.; Liu, H.; Cheng, X.-B.; Yan, C.; Huang, J.-Q. Beyond lithium ion batteries: Higher energy density battery systems based on lithium metal anodes. *Energy Storage Mater.* **2018**, *12*, 161–175. [[CrossRef](#)]
- Natarajan, S.; Aravindan, V. Burgeoning prospects of spent lithium-ion batteries in multifarious applications. *Adv. Energy Mater.* **2018**, *8*, 1802303. [[CrossRef](#)]
- Kim, T.-H.; Park, J.-S.; Chang, S.K.; Choi, S.; Ryu, J.H.; Song, H.-K. The current move of lithium ion batteries towards the next phase. *Adv. Energy Mater.* **2012**, *2*, 860–872. [[CrossRef](#)]
- Nayak, P.K.; Yang, L.; Brehm, W.; Adelhelm, P. From lithium-ion to sodium-ion batteries: Advantages, challenges, and surprises. *Angew. Chem. Int. Ed.* **2018**, *57*, 102–120. [[CrossRef](#)]
- Sun, C.; Zhang, X.; Li, C.; Wang, K.; Sun, X.; Ma, Y. Recent advances in prelithiation materials and approaches for lithium-ion batteries and capacitors. *Energy Storage Mater.* **2020**, *32*, 497–516. [[CrossRef](#)]
- Yu, P.; Zeng, Y.; Zhang, H.; Yu, M.; Tong, Y.; Lu, X. Flexible Zn-ion batteries: Recent progresses and challenges. *Small* **2019**, *15*, e1804760. [[CrossRef](#)]
- Dong, H.; Li, J.; Guo, J.; Lai, F.; Zhao, F.; Jiao, Y.; Brett, D.J.L.; Liu, T.; He, G.; Parkin, I.P. Insights on flexible zinc-ion batteries from lab research to commercialization. *Adv. Mater.* **2021**, *33*, e2007548. [[CrossRef](#)] [[PubMed](#)]

12. Fang, G.; Zhou, J.; Pan, A.; Liang, S. Recent advances in aqueous zinc-ion batteries. *ACS Energy Lett.* **2018**, *3*, 2480–2501. [[CrossRef](#)]
13. Lv, Y.; Xiao, Y.; Ma, L.; Zhi, C.; Chen, S. Recent advances in electrolytes for “beyond aqueous” zinc-ion batteries. *Adv. Mater.* **2022**, *34*, 2106409. [[CrossRef](#)] [[PubMed](#)]
14. Song, Y.; Ruan, P.; Mao, C.; Chang, Y.; Wang, L.; Dai, L.; Zhou, P.; Lu, B.; Zhou, J.; He, Z. Metal-organic frameworks functionalized separators for robust aqueous zinc-ion batteries. *Nano-Micro Lett.* **2022**, *14*, 218. [[CrossRef](#)] [[PubMed](#)]
15. Zeng, Y.; Liang, J.; Zheng, J.; Huang, Z.; Zhang, X.; Zhu, G.; Wang, Z.; Liang, H.; Zhang, Y.-Z. Recent progress in advanced flexible zinc ion battery design. *Appl. Phys. Rev.* **2022**, *9*, 021304. [[CrossRef](#)]
16. Chu, Y.; Ren, L.; Hu, Z.; Huang, C.; Luo, J. An in-depth understanding of improvement strategies and corresponding characterizations towards Zn anode in aqueous Zn-ions batteries. *Green Energy Environ.* **2023**, *8*, 1006–1042. [[CrossRef](#)]
17. Wang, Y.; Sun, S.; Wu, X.; Liang, H.; Zhang, W. Status and opportunities of zinc ion hybrid capacitors: Focus on carbon materials, current collectors, and separators. *Nano-Micro Lett.* **2023**, *15*, 78. [[CrossRef](#)]
18. Wang, T.; Li, C.; Xie, X.; Lu, B.; He, Z.; Liang, S.; Zhou, J. Anode materials for aqueous zinc ion batteries: Mechanisms, properties, and perspectives. *ACS Nano* **2020**, *14*, 16321–16347. [[CrossRef](#)]
19. Aizudin, M.; Fu, W.; Pottammel, R.P.; Dai, Z.; Wang, H.; Rui, X.; Zhu, J.; Li, C.C.; Wu, X.-L.; Ang, E.H. Recent advancements of graphene-based materials for zinc-based batteries: Beyond lithium-ion batteries. *Small* **2023**, *23*, 2305217. [[CrossRef](#)]
20. Zhou, L.F.; Du, T.; Li, J.Y.; Wang, Y.S.; Gong, H.; Yang, Q.R.; Chen, H.; Luo, W.B.; Wang, J.Z. A strategy for anode modification for future zinc-based battery application. *Mater. Horiz.* **2022**, *9*, 2722–2751. [[CrossRef](#)]
21. Chen, R.; Zhang, W.; Huang, Q.; Guan, C.; Zong, W.; Dai, Y.; Du, Z.; Zhang, Z.; Li, J.; Guo, F.; et al. Trace amounts of triple-functional additives enable reversible aqueous zinc-ion batteries from a comprehensive perspective. *Nano-Micro Lett.* **2023**, *15*, 81. [[CrossRef](#)] [[PubMed](#)]
22. Wu, L.; Dong, Y. Recent progress of carbon nanomaterials for high-performance cathodes and anodes in aqueous zinc ion batteries. *Energy Storage Mater.* **2021**, *41*, 715–737. [[CrossRef](#)]
23. Pomerantseva, E.; Bonaccorso, F.; Feng, X.; Cui, Y.; Gogotsi, Y. Energy storage: The future enabled by nanomaterials. *Science* **2019**, *366*, eaan8285. [[CrossRef](#)] [[PubMed](#)]
24. Xu, X.; Xiong, F.; Meng, J.; Wang, X.; Niu, C.; An, Q.; Mai, L. Vanadium-based nanomaterials: A promising family for emerging metal-ion batteries. *Adv. Funct. Mater.* **2020**, *30*, 1904398. [[CrossRef](#)]
25. Zhang, W.; Zuo, C.; Tang, C.; Tang, W.; Lan, B.; Fu, X.; Dong, S.; Luo, P. The Current Developments and Perspectives of V₂O₅ as Cathode for Rechargeable Aqueous Zinc-Ion Batteries. *Energy Technol.* **2020**, *9*, 2000789. [[CrossRef](#)]
26. Zhao, Y.; Zhu, Y.; Zhang, X. Challenges and perspectives for manganese-based oxides for advanced aqueous zinc-ion batteries. *InfoMat* **2019**, *2*, 237–260. [[CrossRef](#)]
27. Shi, L.-N.; Li, X.-Z.; Cui, L.-T.; Wang, P.-F.; Xie, Y.; Yi, T.-F. Recent progresses and perspectives of VN-based materials in the application of electrochemical energy storage. *J. Ind. Eng. Chem.* **2022**, *114*, 52–76. [[CrossRef](#)]
28. Sun, W.; Zhang, Y.; Kang, W.; Deng, N.; Wang, X.; Kang, X.; Yan, Z.; Pan, Y.; Ni, J. Synthesis of MoS₂-based nanostructures and their applications in rechargeable ion batteries, catalysts and gas sensors: A review. *RSC Adv.* **2022**, *12*, 19512–19527. [[CrossRef](#)]
29. Tie, Z.; Niu, Z. Design strategies for high-performance aqueous Zn/organic batteries. *Angew. Chem. Int. Ed. Engl.* **2020**, *59*, 21293–21303. [[CrossRef](#)]
30. Han, C.; Zhu, J.; Zhi, C.; Li, H. The rise of aqueous rechargeable batteries with organic electrode materials. *J. Mater. Chem. A* **2020**, *8*, 15479–15512. [[CrossRef](#)]
31. Tang, Y.; Li, S.; Lin, M.F.; Chen, J.; Eh, A.L.S.; Xu, Q. A π-π Stacked High-Performance Organic Anode for Durable Rocking-Chair Zinc-Ion Battery. *Batteries* **2023**, *9*, 318. [[CrossRef](#)]
32. Wang, J.; Kirlikovali, K.O.; Kim, S.Y.; Kim, D.-W.; Varma, R.S.; Jang, H.W.; Farha, O.K.; Shokouhimehr, M. Metal organic framework-based nanostructure materials: Applications for non-lithium ion battery electrodes. *CrystEngComm* **2022**, *24*, 2925–2947. [[CrossRef](#)]
33. Wang, L.; Zhu, Y.; Du, C.; Ma, X.; Cao, C. Advances and challenges in metal-organic framework derived porous materials for batteries and electrocatalysis. *J. Mater. Chem. A* **2020**, *8*, 24895–24919. [[CrossRef](#)]
34. Zhang, L.; Chen, Y.; Jiang, Z.; Chen, J.; Wei, C.; Wu, W.; Li, S.; Xu, Q. Cation-Anion Redox Active Organic Complex for High Performance Aqueous Zinc Ion Battery. *Energy Environ. Mater.* **2022**, *e12507*. [[CrossRef](#)]
35. Shi, F.; Chen, C.; Xu, Z.-L. Recent advances on electrospun nanofiber materials for post-lithium ion batteries. *Adv. Fiber Mater.* **2021**, *3*, 275–301. [[CrossRef](#)]
36. Yao, H.; Yu, H.; Zheng, Y.; Li, N.W.; Li, S.; Luan, D.; Lou, X.W.; Yu, L. Pre-intercalation of ammonium ions in layered δ-MnO₂ nanosheets for high-performance aqueous zinc-ion batteries. *Angew. Chem. Int. Ed.* **2023**, *62*, e202315257. [[CrossRef](#)]
37. Lu, Y.; Zhu, T.; Bergh, W.V.D.; Stefik, M.; Huang, K. A high performing Zn-ion battery cathode enabled by in situ transformation of V₂O₅ atomic layers. *Angew. Chem.* **2020**, *132*, 17152–17159. [[CrossRef](#)]
38. Zong, Q.; Du, W.; Liu, C.; Yang, H.; Zhang, Q.; Zhou, Z.; Atif, M.; Alsalhi, M.; Cao, G. Enhanced reversible zinc ion intercalation in deficient ammonium vanadated for high-performance aqueous zinc-ion battery. *Nano-Micro Lett.* **2021**, *13*, 116. [[CrossRef](#)]
39. Yan, Y.; Liu, X.; Yan, J.; Guan, C.; Wang, J. Electrospun nanofibers for new generation flexible energy storage. *Energy Environ. Mater.* **2021**, *4*, 502–521. [[CrossRef](#)]
40. Ilango, P.R.; Savariraj, A.D.; Huang, H.; Li, L.; Hu, G.; Wang, H.; Hou, X.; Kim, B.C.; Ramakrishna, S.; Peng, S. Electrospun Flexible Nanofibres for Batteries: Design and Application. *Electrochim. Energy Rev.* **2023**, *6*, 12. [[CrossRef](#)]

41. Zhao, H.; Lam, W.-Y.A.; Ao, K.L.; Xian, Y.; Ren, Y.; Si, L.; Wei, Z.; Wang, J.; Daoud, W.A. Application Progress and Practical Evaluations of Nanofiber Nonwoven Fabrics for Flexible/wearable Batteries. *J. Electrochem. Soc.* **2022**, *169*, 120518. [\[CrossRef\]](#)
42. Joshi, B.; Samuel, E.; Kim, Y.; Yarin, A.L.; Swihart, M.T.; Yoon, S.S. Progress and potential of electrospinning-derived substrate-free and binder-free lithium-ion battery electrodes. *Chem. Eng. J.* **2022**, *430*, 132876. [\[CrossRef\]](#)
43. He, H.; Lian, J.; Chen, C.; Xiong, Q.; Li, C.C.; Zhang, M. Enabling multi-chemisorption sites on carbon nanofibers cathodes by an in-situ exfoliation strategy for high-performance Zn-ion hybrid capacitors. *Nano-Micro Lett.* **2022**, *14*, 106. [\[CrossRef\]](#) [\[PubMed\]](#)
44. Wang, J.; Wang, Z.; Ni, J.; Li, L. Electrospinning for flexible sodium-ion batteries. *Energy Storage Mater.* **2022**, *45*, 704–719. [\[CrossRef\]](#)
45. Wang, Y.; Liu, Y.; Liu, Y.; Shen, Q.; Chen, C.; Qiu, F.; Li, P.; Jiao, L.; Qu, X. Recent advances in electrospun electrode materials for sodium-ion batteries. *J. Energy Chem.* **2021**, *54*, 225–241. [\[CrossRef\]](#)
46. Xia, C.; Zhou, Y.; He, C.; Douka, A.I.; Guo, W.; Qi, K.; Xia, B.Y. Recent advances on electrospun nanomaterials for zinc-air batteries. *Small Sci.* **2021**, *1*, 2100010. [\[CrossRef\]](#)
47. Lu, X.; Wang, C.; Favier, F.; Pinna, N. Electrospun nanomaterials for supercapacitor electrodes: Designed architectures and electrochemical performance. *Adv. Energy Mater.* **2017**, *7*, 1601301. [\[CrossRef\]](#)
48. Liang, J.; Zhao, H.; Yue, L.; Fan, G.; Li, T.; Lu, S.; Chen, G.; Gao, S.; Asiri, A.M.; Sun, X. Recent advances in electrospun nanofibers for supercapacitors. *J. Mater. Chem. A* **2020**, *8*, 16747–16789. [\[CrossRef\]](#)
49. Inagaki, M.; Yang, Y.; Kang, F. Carbon nanofibers prepared via electrospinning. *Adv. Mater.* **2012**, *24*, 2547–2566. [\[CrossRef\]](#)
50. Guo, Y.; Wang, X.; Shen, Y.; Dong, K.; Shen, L.; Alzalab, A.A.A. Research progress, models and simulation of electrospinning technology: A review. *J. Mater. Sci.* **2022**, *57*, 58–104. [\[CrossRef\]](#)
51. Medeiros, G.B.; Lima, F.A.; de Almeida, D.S.; Guerra, V.G.; Aguiar, M.L. Modification and functionalization of fibers formed by electrospinning: A review. *Membranes* **2022**, *12*, 861. [\[CrossRef\]](#) [\[PubMed\]](#)
52. Teo, W.E.; Ramakrishna, S. A review on electrospinning design and nanofibre assemblies. *Nanotechnology* **2006**, *17*, 89–106. [\[CrossRef\]](#) [\[PubMed\]](#)
53. He, J.-H. On the height of Taylor cone in electrospinning. *Results. Phys.* **2020**, *17*, 103096. [\[CrossRef\]](#)
54. Hsu, P.-C.; Wang, S.; Wu, H.; Narasimhan, V.K.; Kong, D.; Ryoung Lee, H.; Cui, Y. Performance enhancement of metal nanowire transparent conducting electrodes by mesoscale metal wires. *Nat. Commun.* **2013**, *4*, 2522. [\[CrossRef\]](#) [\[PubMed\]](#)
55. Frank, E.; Steudle, L.M.; Ingildeev, D.; Spörl, J.M.; Buchmeiser, M.R. Carbon fibers: Precursor systems, processing, structure, and properties. *Angew. Chem. Int. Ed.* **2014**, *53*, 5262–5298. [\[CrossRef\]](#) [\[PubMed\]](#)
56. Li, K.; Ni, X.; Wu, Q.; Yuan, C.; Li, C.; Li, D.; Chen, H.; Lv, Y.; Ju, A. Carbon-Based Fibers: Fabrication, Characterization and Application. *Adv. Fiber Mater.* **2022**, *4*, 631–682. [\[CrossRef\]](#)
57. Wang, X.; Li, Y.; Wang, S.; Zhou, F.; Das, P.; Sun, C.; Zheng, S.; Wu, Z.-S. 2D Amorphous V₂O₅/Graphene Heterostructures for High-Safety Aqueous Zn-Ion Batteries with Unprecedented Capacity and Ultrahigh Rate Capability. *Adv. Energy Mater.* **2020**, *10*, 2000081. [\[CrossRef\]](#)
58. Deng, S.; Yuan, Z.; Tie, Z.; Wang, C.; Song, L.; Niu, Z. Electrochemically Induced Metal–Organic-Framework-Derived Amorphous V₂O₅ for Superior Rate Aqueous Zinc-Ion Batteries. *Angew. Chem. Int. Ed.* **2020**, *59*, 22002–22006. [\[CrossRef\]](#)
59. Li, Z.; Ganapathy, S.; Xu, Y.; Zhou, Z.; Sarilar, M.; Wagemaker, M. Mechanistic Insight into the Electrochemical Performance of Zn/VO₂ Batteries with an Aqueous ZnSO₄ Electrolyte. *Adv. Energy Mater.* **2019**, *9*, 1900237. [\[CrossRef\]](#)
60. Liu, Y.; Hu, P.; Liu, H.; Wu, X.; Zhi, C. Tetragonal VO₂ hollow nanospheres as robust cathode material for aqueous zinc ion batteries. *Mater. Today Energy* **2020**, *17*, 100431. [\[CrossRef\]](#)
61. Yang, Y.; Tang, Y.; Liang, S.; Wu, Z.; Fang, G.; Cao, X.; Wang, C.; Lin, T.; Pan, A.; Zhou, J. Transition metal ion-preintercalated V₂O₅ as high-performance aqueous zinc-ion battery cathode with broad temperature adaptability. *Nano Energy* **2019**, *61*, 617–625. [\[CrossRef\]](#)
62. Ren, X.; Liu, H.; Wang, N.; Hu, L.; Sun, M.; Bo, L.; Li, Z.; Jia, C. Dual Pre-Insertion Strategy to Achieve High-Performance Vanadium Oxide toward Advanced Cylindrical Zinc Ion Batteries. *ACS Sustain. Chem. Eng.* **2023**, *11*, 16965–16974. [\[CrossRef\]](#)
63. Zhang, X.; Bian, R.; Sang, Z.; Tan, S.; Liang, J.; Wang, L.; Hou, F. Anion and Cation Co-Modified Vanadium Oxide for Cathode Material of Aqueous Zinc-Ion Battery. *Batteries* **2023**, *9*, 352. [\[CrossRef\]](#)
64. Song, Y.; Jing, L.; Wang, R.; Cui, J.; Li, M.; Zhang, Y. Vanadium oxide nanospheres encapsulated in N-doped carbon nanofibers with morphology and defect dual-engineering toward advanced aqueous zinc-ion batteries. *J. Energy Chem.* **2024**, *89*, 599–609. [\[CrossRef\]](#)
65. Zheng, C.; Huang, Z.H.; Sun, F.F.; Zhang, Y.; Li, H.; Liu, Y.; Ma, T. Oxygen-Vacancy-Reinforced Vanadium Oxide/Graphene Heterojunction for Accelerated Zinc Storage with Long Life Span. *Small* **2023**, *2306275*. [\[CrossRef\]](#) [\[PubMed\]](#)
66. Xu, N.; Yan, C.; He, W.; Xu, L.; Jiang, Z.; Zheng, A.; Wu, H.; Chen, M.; Diao, G. Flexible electrode material of V₂O₅ carbon fiber cloth for enhanced zinc ion storage performance in flexible zinc-ion battery. *J. Power Source* **2022**, *533*, 231358. [\[CrossRef\]](#)
67. Wang, H.; Zhang, S.; Deng, C. In Situ Encapsulating Metal Oxides into Core–Shell Hierarchical Hybrid Fibers for Flexible Zinc-Ion Batteries toward High Durability and Ultrafast Capability for Wearable Applications. *Acad Appl. Mater. Inter.* **2019**, *11*, 35796–35808. [\[CrossRef\]](#)
68. Chen, Z.; Hu, J.; Liu, S.; Hou, H.; Zou, G.; Deng, W.; Ji, X. Dual defects boosting zinc ion storage of hierarchical vanadium oxide fibers. *Chem. Eng. J.* **2021**, *404*, 126536. [\[CrossRef\]](#)

69. Chen, X.; Wang, L.; Li, H.; Cheng, F.; Chen, J. Porous V₂O₅ nanofibers as cathode materials for rechargeable aqueous zinc-ion batteries. *J. Energy Chem.* **2019**, *38*, 20–25. [[CrossRef](#)]
70. Yoo, G.; Ryu, G.H.; Koo, B.-R.; An, G.-H. Interfacial defect engineering via combusted graphene in V₂O₅ nanochips to develop high-rate and stable zinc-ion batteries. *Ceram. Int.* **2021**, *47*, 31817–31825. [[CrossRef](#)]
71. Yoo, G.; Koo, B.-R.; An, H.-R.; Huang, C.; An, G.-H. Enhanced and stabilized charge transport boosting by Fe-doping effect of V₂O₅ nanorod for rechargeable Zn-ion battery. *J. Ind. Eng. Chem.* **2021**, *99*, 344–351. [[CrossRef](#)]
72. Yan, M.; He, P.; Chen, Y.; Wang, S.; Wei, Q.; Zhao, K.; Xu, X.; An, Q.; Shuang, Y.; Shao, Y.; et al. Water-Lubricated Intercalation in V₂O₅·nH₂O for High-Capacity and High-Rate Aqueous Rechargeable Zinc Batteries. *Adv. Mater.* **2018**, *30*, 1703725. [[CrossRef](#)] [[PubMed](#)]
73. Liu, J.; Zhan, L.; Sun, K.; Huang, K.; Wei, T.; Wang, C. Electrospinning Preparation of a High-Rate Self-Supported Cathode for Rechargeable Aqueous Zinc-Ion Batteries. *Energy Fuel* **2022**, *36*, 13278–13285. [[CrossRef](#)]
74. Liu, X.; Wang, Z.; Niu, Y.; Liu, C.; Chen, H.; Ren, X.; Liu, Z.; Lau, W.-M.; Zhou, D. Electrospun V₂O₃@Carbon Nanofibers as a Flexible and Binder-Free Cathode for Highly Stable Aqueous Zn-Ion Full Batteries. *ACS Appl. Energy Mater.* **2022**, *5*, 3525–3535. [[CrossRef](#)]
75. Tan, H.; Feng, Y.; Rui, X.; Yu, Y.; Huang, S. Metal chalcogenides: Paving the way for high-performance sodium/potassium-ion batteries. *Small Methods* **2020**, *4*, 1900563. [[CrossRef](#)]
76. Yang, W.; Chen, D.; She, Y.; Zeng, M.; Lin, X.; Ang, E.H.; Yan, C.; Qin, Y.; Rui, X. Rational design of vanadium chalcogenides for sodium-ion batteries. *J. Power Source* **2020**, *478*, 228769. [[CrossRef](#)]
77. Yang, J.; Yang, H.; Ye, C.; Li, T.; Chen, G.; Qiu, Y. Conformal surface-nanocoating strategy to boost high-performance film cathodes for flexible zinc-ion batteries as an amphibious soft robot. *Energy Storage Mater.* **2022**, *46*, 472–481. [[CrossRef](#)]
78. Hu, Y.; Zhang, Y.; Zhu, J.; Niu, Z. Rational design of continuous gradient composite films for high-performance zinc-ion batteries. *Energy Storage Mater.* **2022**, *51*, 382–390. [[CrossRef](#)]
79. Nolis, G.M.; Adil, A.; Yoo, H.D.; Hu, L.; Bayliss, R.D.; Lapidus, S.H.; Berkland, L.; Phillips, P.J.; Freeland, J.W.; Kim, C.; et al. Electrochemical Reduction of a Spinel-Type Manganese Oxide Cathode in Aqueous Electrolytes with Ca²⁺ or Zn²⁺. *J. Phys. Chem. C* **2018**, *122*, 4182–4188. [[CrossRef](#)]
80. Gao, X.; Wu, H.; Li, W.; Tian, Y.; Zhang, Y.; Wu, H.; Yang, L.; Zou, G.; Hou, H.; Ji, X. H⁺-Insertion Boosted α-MnO₂ for an Aqueous Zn-Ion Battery. *Small* **2020**, *16*, 1905842. [[CrossRef](#)]
81. Zhang, D.; Cao, J.; Zhang, X.; Insin, N.; Wang, S.; Han, J.; Zhao, Y.; Qin, J.; Huang, Y. Inhibition of Manganese Dissolution in Mn₂O₃ Cathode with Controllable Ni²⁺ Incorporation for High-Performance Zinc Ion Battery. *Adv. Funct. Mater.* **2021**, *31*, 2009412. [[CrossRef](#)]
82. Tan, Q.; Li, X.; Zhang, B.; Chen, X.; Tian, Y.; Wan, H.; Zhang, L.; Miao, L.; Wang, C.; Gan, Y.; et al. Valence Engineering via In Situ Carbon Reduction on Octahedron Sites Mn₃O₄ for Ultra-Long Cycle Life Aqueous Zn-Ion Battery. *Adv. Energy Mater.* **2020**, *10*, 2001050. [[CrossRef](#)]
83. Guo, D.; Zhao, W.; Pan, F.; Liu, G. Block Copolymer-Derived Porous Carbon Fibers Enable High MnO₂ Loading and Fast Charging in Aqueous Zinc-Ion Batter. *Supercaps* **2022**, *5*, e2021003801. [[CrossRef](#)]
84. Fang, L.; Wang, X.; Shi, W.; Le, Z.; Wang, H.; Nie, P.; Xu, T.; Chang, L. Carbon nanofibers enabling manganese oxide cathode superior low temperature performance for aqueous zinc-ion batteries. *J. Electroanal. Chem.* **2023**, *940*, 117488. [[CrossRef](#)]
85. Tang, F.; Wu, X.; Shen, Y.; Xiang, Y.; Wu, X.; Xiong, L.; Wu, X. The intercalation cathode materials of heterostructure MnS/MnO with dual ions defect embedded in N-doped carbon fibers for aqueous zinc ion batteries. *Energy Storage Mater.* **2022**, *52*, 180–188. [[CrossRef](#)]
86. Tang, F.; He, T.; Zhang, H.; Wu, X.; Li, Y.; Long, F.; Xiang, Y.; Zhu, L.; Wu, J.; Wu, X. The MnO@N-doped carbon composite derived from electrospinning as cathode material for aqueous zinc ion battery. *J. Electroanal. Chem.* **2020**, *873*, 114368. [[CrossRef](#)]
87. Yang, J.; Yao, G.; Li, Z.; Zhang, Y.; Wei, L.; Niu, H.; Chen, Q.; Zheng, F. Highly Flexible K-Intercalated MnO₂/Carbon Membrane for High-Performance Aqueous Zinc-Ion Battery Cathode. *Small* **2023**, *19*, e2205544. [[CrossRef](#)]
88. Long, J.; Yang, Z.; Yang, F.; Cuan, J.; Wu, J. Electrospun core-shell Mn₃O₄/carbon fibers as high-performance cathode materials for aqueous zinc-ion batteries. *Electrochim. Acta* **2020**, *344*, 136155. [[CrossRef](#)]
89. Cheng, L.; Wu, Y.; Guo, S.; Liu, Y.; Li, W.; Liu, Q.; Mo, F.; Yu, S.; Huang, Y.; Wei, J. Electrospun manganese sesquioxide as cathode for aqueous zinc ion battery with high-rate performance and long cycle life. *Mater. Lett.* **2022**, *327*, 132920. [[CrossRef](#)]
90. Zhao, Y.; Huang, Y.; Wu, F.; Chen, R.; Li, L. High-Performance Aqueous Zinc Batteries Based on Organic/Organic Cathodes Integrating Multiredox Centers. *Adv. Mater.* **2021**, *33*, 2106469. [[CrossRef](#)]
91. Kim, C.; Ahn, B.Y.; Wei, T.S.; Jo, Y.; Jeong, S.; Choi, Y.; Kim, I.D.; Lewis, J.A. High-power aqueous zinc-ion batteries for customized electronic devices. *ACS Nano* **2018**, *12*, 11838–11846. [[CrossRef](#)] [[PubMed](#)]
92. Liu, M.; Li, X.; Shao, C.; Han, C.; Liu, Y.; Li, X.; Ma, X.; Chen, F.; Liu, Y. Synchronous-ultrahigh conductive-reactive N-atoms doping strategy of carbon nanofibers networks for high-performance flexible energy storage. *Energy Storage Mater.* **2022**, *44*, 250–262. [[CrossRef](#)]
93. Cai, Z.; Guo, J.; Yang, H.; Xu, Y. Electrochemical properties of electrospun poly (5-cyanoindole) submicron-fibrous electrode for zinc/polymer secondary battery. *J. Power Source* **2015**, *279*, 114–122. [[CrossRef](#)]
94. Ren, Q.; Wang, H.; Lu, X.-F.; Tong, Y.-X.; Li, G.-R. Recent progress on MOF-derived heteroatom-doped carbon-based electrocatalysts for oxygen reduction reaction. *Adv. Sci.* **2018**, *5*, 1700515. [[CrossRef](#)] [[PubMed](#)]

95. Yu, J.; Cai, D.; Si, J.; Zhan, H.; Wang, Q. MOF-derived NiCo₂S₄ and carbon hybrid hollow spheres compactly concatenated by electrospun carbon nanofibers as self-standing electrodes for aqueous alkaline Zn batteries. *J. Mater. Chem. A* **2022**, *10*, 4100–4109. [[CrossRef](#)]
96. Zhang, Y.; Jiang, S.; Li, Y.; Ren, X.; Zhang, P.; Sun, L.; Yang, H.Y. In Situ Grown Hierarchical Electrospun Nanofiber Skeletons with Embedded Vanadium Nitride Nanograins for Ultra-Fast and Super-Long Cycle Life Aqueous Zn-Ion Batteries. *Adv. Energy Mater.* **2022**, *13*, 2202826. [[CrossRef](#)]
97. Ding, L.; Gao, J.; Yan, T.; Cheng, C.; Chang, L.Y.; Zhang, N.; Feng, X.; Zhang, L. Boosting the Cycling Stability of Aqueous Zinc-Ion Batteries through Nanofibrous Coating of a Bead-like MnO_x Cathode. *ACS Appl. Mater. Inter.* **2022**, *14*, 17570–17577. [[CrossRef](#)]
98. Du, W.; Ang, E.H.; Yang, Y.; Zhang, Y.; Ye, M.; Li, C.C. Challenges in the material and structural design of zinc anode towards high-performance aqueous zinc-ion batteries. *Energy Environ. Sci.* **2020**, *13*, 3330–3360. [[CrossRef](#)]
99. Zhou, M.; Guo, S.; Li, J.; Luo, X.; Liu, Z.; Zhang, T.; Cao, X.; Long, M.; Lu, B.; Pan, A.; et al. Surface-preferred crystal plane for a stable and reversible zinc anode. *Adv. Mater.* **2021**, *33*, 2100187. [[CrossRef](#)]
100. Zhang, Q.; Luan, J.; Huang, X.; Wang, Q.; Sun, D.; Tang, Y.; Ji, X.; Wang, H. Revealing the role of crystal orientation of protective layers for stable zinc anode. *Nat. Commun.* **2020**, *11*, 3961. [[CrossRef](#)]
101. Zhang, Q.; Luan, J.; Fu, L.; Wu, S.; Tang, Y.; Ji, X.; Wang, H. The three-dimensional dendrite-free zinc anode on a copper mesh with a zinc-oriented polyacrylamide electrolyte additive. *Angew. Chem. Int. Ed.* **2019**, *58*, 15841–15847. [[CrossRef](#)] [[PubMed](#)]
102. Zhao, Z.; Zhao, J.; Hu, Z.; Li, J.; Li, J.; Zhang, Y.; Wang, C.; Cui, G. Long-life and deeply rechargeable aqueous Zn anodes enabled by a multifunctional brightener-inspired interphase. *Energy Environ. Sci.* **2019**, *12*, 1938–1949. [[CrossRef](#)]
103. Li, G.; Yang, Z.; Jiang, Y.; Jin, C.; Huang, W.; Ding, X.; Huang, Y. Towards polyvalent ion batteries: A zinc-ion battery based on NASICON structured Na₃V₂(PO₄)₃. *Nano Energy* **2016**, *25*, 211–217. [[CrossRef](#)]
104. Kumar, S.; Yoon, H.; Park, H.; Park, G.; Suh, S.; Kim, H.-J. A dendrite-free anode for stable aqueous rechargeable zinc-ion batteries. *J. Ind. Eng. Chem.* **2022**, *108*, 321–327. [[CrossRef](#)]
105. Park, G.; Park, H.; Seol, W.; Suh, S.; Jo, J.Y.; Kumar, S.; Kim, H.J. Inhibition of Zinc Dendrites Realized by a β-P(VDF-TrFE) Nanofiber Layer in Aqueous Zn-Ion Batteries. *Membranes* **2022**, *12*, 1014. [[CrossRef](#)] [[PubMed](#)]
106. Jian, Q.; Wan, Y.; Sun, J.; Wu, M.; Zhao, T. A dendrite-free zinc anode for rechargeable aqueous batteries. *J. Mater. Chem. A* **2020**, *8*, 20175–20184. [[CrossRef](#)]
107. Li, H.; Han, C.; Huang, Y.; Huang, Y.; Zhu, M.; Pei, Z.; Xue, Q.; Wang, Z.; Liu, Z.; Tang, Z.; et al. An extremely safe and wearable solid-state zinc ion battery based on a hierarchical structured polymer electrolyte. *Energy Environ. Sci.* **2018**, *11*, 941–951. [[CrossRef](#)]
108. Liu, Q.; Wang, Y.; Hong, X.; Zhou, R.; Hou, Z.; Zhang, B. Elastomer-Alginate Interface for High-Power and High-Energy Zn Metal Anodes. *Adv. Energy Mater.* **2022**, *12*, 2200318. [[CrossRef](#)]
109. Liang, Y.; Wang, Y.; Mi, H.; Sun, L.; Ma, D.; Li, H.; He, C.; Zhang, P. Functionalized carbon nanofiber interlayer towards dendrite-free, Zn-ion batteries. *Chem. Eng. J.* **2021**, *425*, 131862. [[CrossRef](#)]
110. Wan, F.; Hao, Z.; Wang, S.; Ni, Y.; Zhu, J.; Tie, Z.; Bi, S.; Niu, Z.; Chen, J. A Universal Compensation Strategy to Anchor Polar Organic Molecules in Bilayered Hydrated Vanadates for Promoting Aqueous Zinc-Ion Storage. *Adv. Mater.* **2021**, *33*, e2102701. [[CrossRef](#)]
111. Yang, S.; Li, Y.; Du, H.; Liu, Y.; Xiang, Y.; Xiong, L.; Wu, X.; Wu, X. Copper nanoparticle-modified carbon nanofiber for seeded zinc deposition enables stable Zn metal anode. *Acs Sustain. Chem. Eng.* **2022**, *10*, 12630–12641. [[CrossRef](#)]
112. Baek, S.H.; Cho, Y.J.; Park, J.M.; Xiong, P.; Yeon, J.S.; Rana, H.H.; Park, J.H.; Jang, G.; Lee, S.J.; Park, H.S. Electrospun conductive carbon nanofiber hosts for stable zinc metal anode. *Int. J. Energy Res.* **2022**, *46*, 7201–7214. [[CrossRef](#)]
113. Yu, H.; Zeng, Y.; Li, N.W.; Luan, D.; Yu, L.; Lou, X.W. Confining Sn nanoparticles in interconnected N-doped hollow carbon spheres as hierarchical zincophilic fibers for dendrite-free Zn metal anodes. *Sci. Adv.* **2022**, *8*, eabm5766. [[CrossRef](#)] [[PubMed](#)]
114. Yang, J.-L.; Yang, P.; Yan, W.; Zhao, J.-W.; Fan, H.J. 3D zincophilic micro-scaffold enables stable Zn deposition. *Energy Storage Mater.* **2022**, *51*, 259–265. [[CrossRef](#)]
115. Zeng, Y.; Sun, P.X.; Pei, Z.; Jin, Q.; Zhang, X.; Yu, L.; Lou, X.W.D. Nitrogen-Doped Carbon Fibers Embedded with Zincophilic Cu Nanoboxes for Stable Zn-Metal Anodes. *Adv. Mater.* **2022**, *34*, e2200342. [[CrossRef](#)] [[PubMed](#)]
116. Cui, J.; Yin, P.; Xu, A.N.; Jin, B.W.; Li, Z.H.; Shao, M.F. Fluorine enhanced nucleophilicity of TiO₂ nanorod arrays: A general approach for dendrite-free anodes towards high-performance metal batteries. *Nano Energy* **2022**, *93*, 106837. [[CrossRef](#)]
117. Xue, P.; Sun, C.; Li, H.P.; Liang, J.J.; Lai, C. Superlithiophilic Amorphous SiO₂-TiO₂ Distributed into Porous Carbon Skeleton Enabling Uniform Lithium Deposition for Stable Lithium Metal Batteries. *Adv. Sci.* **2019**, *6*, 1900943. [[CrossRef](#)]
118. Song, Y.; Chen, Y.; Wang, Z.; Zhao, W.; Qin, C.; Yu, H.; Wang, X.; Bakenov, Z.; Zhang, Y. Defective ZnO_x@porous carbon nanofiber network inducing dendrite-free zinc plating as zinc metal anode for high-performance aqueous rechargeable Zn/Na₄Mn₉O₁₈ battery based on hybrid electrolyte. *J. Power Source* **2022**, *518*, 230761. [[CrossRef](#)]
119. Xue, P.; Guo, C.; Wang, N.; Zhu, K.; Jing, S.; Kong, S.; Zhang, X.; Li, L.; Li, H.; Feng, Y.; et al. Synergistic Manipulation of Zn²⁺ Ion Flux and Nucleation Induction Effect Enabled by 3D Hollow SiO₂/TiO₂/Carbon Fiber for Long-Lifespan and Dendrite-Free Zn-Metal Composite Anodes. *Adv. Funct. Mater.* **2021**, *31*, 2106417. [[CrossRef](#)]